

REx: Data-Free Residual Quantization Error Expansion

Edouard Yvinec^{1,2} Arnaud Dapogny¹ Matthieu Cord² Kevin Bailly^{1,2}

Abstract

Deep neural networks (DNNs) are ubiquitous in computer vision and natural language processing, but suffer from high inference cost. This problem can be addressed by quantization, which consists in converting floating point operations into a lower bit-width format. With the growing concerns on privacy rights, we focus our efforts on data-free methods. However, such techniques suffer from their lack of adaptability to the target devices, as a hardware typically only support specific bit widths. Thus, to adapt to a variety of devices, a quantization method shall be flexible enough to find good accuracy *v.s.* speed trade-offs for every bit width and target device. To achieve this, we propose REx, a quantization method that leverages residual error expansion, along with group sparsity and an ensemble approximation for better parallelization. REx is backed off by strong theoretical guarantees and achieves superior performance on every benchmarked application (from vision to NLP tasks), architecture (ConvNets, transformers) and bit-width (from int8 to ternary quantization).

1. Introduction

Deep neural networks (DNNs) achieve outstanding performance on several challenging computer vision tasks such as image classification (He et al., 2016), object detection (Liu et al., 2016) and semantic segmentation (Chen et al., 2017) as well as natural language processing benchmarks such as text classification (Devlin et al., 2018). However, their accuracy comes at a high computational inference cost which limits their deployment, moreso on edge devices when real-time treatment as well as energy consumption are a concern. This problem can be tackled *via* DNN quantization, *i.e.* by reducing the bit-width representation of the com-

^{*}Equal contribution ¹Datakalab, 114 boulevard Malesherbes, 75017 Paris, France ²Sorbonne Université, CNRS, ISIR, f-75005, 4 Place Jussieu 75005 Paris, France. Correspondence to: Edouard Yvinec <ey@datakalab.com>.

putations from floating point operations (FP) to e.g. int8 (8-bits integer representation), int4, int3 or even lower-bit representation such as ternary (where weights values are either -1 , 0 or $+1$) quantization. Because DNN inference principally relies on matrix multiplication, such quantization dramatically diminishes the number of bit-wise operations (as defined by Krishnamoorthi 2018), thus limiting the DNN latency and energy consumption. However, DNN quantization usually comes at the expense of the network accuracy. As a consequence, DNN quantization is an active field of research (Courbariaux et al., 2016; Wu et al., 2018; Jacob et al., 2018; Achterhold et al., 2018; Louizos et al., 2018; Sheng et al., 2018; Choi et al., 2022; Zhong et al., 2022) that aims at limiting this accuracy drop while reducing the number of bit-wise operations.

All the aforementioned methods are data-driven as they either involve training a network from scratch or fine-tune an already trained and quantized one. However, while such approaches usually allow lower quantization errors using low bit-wise representations, due to the growing concerns on privacy rights and data privacy, there is a growing number of real-case scenarios (e.g. health and military services) where data may not be available for quantization purposes. Motivated by these observations, several data-free quantization algorithms were published in the recent years (Nagel et al., 2019; Meller et al., 2019; Zhao et al., 2019; Cai et al., 2020; Zhang et al., 2021; Cong et al., 2022), which focus on the quantization operator, *i.e.* the transformation which maps the floating point weights to their low-bit, fixed point, values. However, these approaches still struggle to offer an interesting alternative to data-driven techniques in terms of accuracy.

Furthermore, when considering a specific target device for deployment, traditional quantization methods, usually focusing on the quantization operator, offer limited options: given a supported bit width (given by the device, as most hardware usually support only a few representation formats (Nvidia, 2021)) they either achieve satisfactory accuracy or not. To address this concern, we wish to design a flexible quantization method, *i.e.* one that can provide several accuracy *vs.* speed trade-off points for each bit width. Drawing inspiration from wavelets-based methods for image compression (Rabbani, 2002; Mallat, 2009), we tackle this limitation by considering the successive residual quan-

ization errors between the quantized and original model. Increasing the number of residuals in the expansion (*i.e.* the expansion order) increases the fidelity to the original, non-quantized model at the expense of additional computations. In addition, we propose a group-sparse expansion which allows us to maintain the accuracy using significantly less bit operations, as well as an ensemble approximation that allows us to better leverage parallelization of the computations. Hence, given a target device, our approach allows to find the best accuracy *vs.* speed trade-offs. Our contributions are thus three-fold:

- **REx, a data-free quantization method that is both efficient and flexible.** REx leverages residual quantization, along with group-sparsity and ensemble approximation to enable finding suitable trade-offs depending on a target bit-width and parallelization capacity.
- **Theoretical guarantees** on both the exponential convergence of the quantized model towards the full-precision model, and ensemble approximation errors. This is of paramount importance in a data-free context, where we cannot easily measure the accuracy degradation.
- **Extensive empirical validation** we show through a thorough empirical validation that REx both significantly outperforms every state-of-the-art data-free quantization technique as a standalone method but also helps improve said methods when used in combination. In particular, REx achieves outstanding performances on both standard and low bit range quantization on various ConvNet architectures applied to ImageNet classification, Pascal VOC object detection, CityScapes semantic segmentation as well as transformers on GLUE text classification.

In addition, REx is agnostic to the quantization operator and can be combined with most recent state-of-the-art methods that focus on the latter.

2. Related Work

2.1. Quantization

In this section, we review existing methods for DNN quantization, with an emphasis on approaches geared towards run-time acceleration rather than memory footprint reduction (*e.g.* methods that only quantize weights [Chen et al. 2015](#); [Gong et al. 2014](#); [Han et al. 2016](#); [Zhou et al. 2017](#)). The vast majority of DNN quantization techniques rely on data usage. Such data-driven approaches can be classified in two main categories. First, methods that involve training a model from scratch, *i.e.* quantization aware training, ([Wu et al., 2018](#); [Jacob et al., 2018](#); [Achterhold et al.,](#)

[2018](#); [Louizos et al., 2018](#); [Sheng et al., 2018](#); [Ullrich et al., 2017](#); [Zhou et al., 2016](#)) usually rely on defining a discrete version of stochastic gradient descent training, typically making use of two distinct models during training: one model with floating-point weight values and a standard training protocol, and a second model with quantized weight updates derived from the first model. Remarkably, [Courbariaux et al. \(2016\)](#) pushed such quantization methods to deal with very low-bit representation by training Binary Neural Networks, essentially on toy tasks. Another class of data-driven methods ([Han et al., 2016](#); [Zhou et al., 2017](#)) rely on fine-tuning a previously trained and quantized DNN. For instance, [Zhou et al. \(2017\)](#) propose to progressively freeze and quantize a portion of the weights while training the remaining floating-point ones. [Oh et al. \(2021\)](#) minimize the residual error during training, using weight decay over the residue. This method is similar with REx insofar as it uses a second order expansion of the quantization errors. However, it discards the quantization error after training while we propose to keep the extra operations in order to ensure a high fidelity to the provided pre-trained model.

2.2. Data-Free Quantization

[Nagel et al. \(2019\)](#) discuss the necessity to have data available so as to successfully design a quantization pipeline. The proposed method consists in balancing the weight ranges over the different layers of a model, using scale invariance properties (similarly to [Stock et al. 2019](#)) that are specific to piece-wise affine (*e.g.* ReLU) activation functions, and relying on a traditional, naive quantization operator ([Krishnamoorthi, 2018](#)). The authors note that the magnitude of the quantization error strongly varies with the DNN architecture: as such, already compact architectures such as MobileNets ([Sandler et al., 2018](#)) appear as challenging for data-free quantization purposes (for instance, [Krishnamoorthi \(2018\)](#) report a dramatic drop to chance-level accuracy without fine-tuning). [Lin et al. \(2016\)](#) studied the properties of the noise induced by the quantization operator. These properties were later used in SQNR ([Meller et al., 2019](#)), a method that consists in assigning, for each layer, an optimal bit-width representation. In the current state of data-free quantization research, we see two major trends: methods that focus on the quantization process itself ([Cong et al., 2022](#); [Yvinec et al., 2023](#)) and methods that focus on generating synthetic data ([Li et al., 2021b](#); [Choi et al., 2022](#); [Zhong et al., 2022](#)). Overall, data-free approaches generally struggle to deal with low-bit representation problem, *i.e.* performing quantization into bit widths lower than int4 (*e.g.* int3 or ternary quantization) and offer very few options when the target device only supports such low-bit values. While the latter usually achieves higher accuracy, the resulting pre-processing is significantly slowed

down: going from a few seconds for (Cong et al., 2022) to a few days for (Li et al., 2021b). With REx, we successfully addresses these challenges with the addition of the residual errors through expansions without using any synthetic data.

2.3. Flexibility in Quantization

In practice, the existing data-free quantization methods only offer a single possible quantized model given a supported bit-width. Nevertheless, most hardwares do not support a wide range of bit-width. For instance, Turing (Feng et al., 2021) and Untether (Robinson, 2022) architectures support int4 and int8 quantization while the Nvidia A100 (Nvidia, 2021) supports int8, int4 and binary (int1) quantization. Worse, in some scenario, the target device may support only one bit-width, e.g. Cognix 0 chip only supports int4 quantization. In such situations, if the quantization operator does not achieve satisfactory accuracy, then no compression shall be performed under the data-free paradigm. Conversely, REx circumvents this limitation by offering several trade-offs given a bit-width representation.

As discussed by Zhang et al. (2022), hardware cost is for the most part derived from energy consumption. This assertion holds for both micro chips and large scale hardware such has high-end GPUs. For this reason quantization is of great relevance even on most recent GPUs which include dedicated cores for integer arithmetic (Nvidia, 2021). As stated by Zhang et al. (2022), quantizing a deep neural network on a GPU provides more benefits than upgrading a GPU by one or even two generations. For these reasons, we assume that large-scale parallelization should not be overlooked in quantization as it bears importance on large devices. Consequently, a flexible quantization method shall provide solutions to facilitate parallel computing when available (quantization for GPUs) in addition to handling devices not benefiting from it (e.g. micro controller units). For that matter, we propose to approximate a network residual expansion as an ensemble.

2.4. Ensemble Methods

Ensemble methods (Dietterich, 2000) are widely studied models in the machine learning community, where weak, yet complimentary predictors are aggregated *via* e.g. bagging (Breiman, 1996), boosting (Friedman et al., 2000) or gradient boosting (Breiman, 1997), to achieve superior performance. Leveraging deep learning and ensemble methods crossovers in order to achieve faster inference through parallelization of smaller models is still an overlooked subject. Nevertheless, some methods leveraged deep ensembles to great success. Of particular interest is the work of Zhu et al. (2019) which consists in learning ensembles of binary neural networks (BNNs) to reach interesting accuracy vs. inference speed trade-offs. However, the accuracy

of the BNN ensembles is significantly lower than that of the full-precision model and are admittedly unstable as the ensembles grow, which the authors attribute to overfitting. REx, however, is robust to such problems while maintaining the inference benefits from ensembling in quantization.

3. Methodology

Let's consider F , a trained network with L layers and trained weights W_l . Given a target integer representation in b bits, e.g. int8 or int4, we consider a quantization operator Q . Formally, Q maps $[\min\{W_l\}; \max\{W_l\}] \subset \mathbb{R}$ to the quantized interval $[-2^{b-1}; 2^{b-1} - 1] \cap \mathbb{Z}$. The most straightforward way to do so is to apply a scaling s_l and round $\lfloor \cdot \rfloor$ the scaled tensor, *i.e.*:

$$Q(W_l) = \left\lfloor \frac{W_l}{s_l} \right\rfloor \quad (1)$$

With s_l the quantization scale for layer l . Following the standard formulation (Gholami et al., 2021), a quantization operator Q , comes with a de-quantization operator Q^{-1} . For the simple quantization operator Q in Equation (1), a natural choice is $Q^{-1}(Q(W_l)) = s_l \times Q(W_l)$. Note that, despite the notation, Q^{-1} is not a true inverse, as by definition of the quantized space, there is some information loss. This loss, called the quantization error, is defined as: $W_l - Q^{-1}(Q(W_l))$. In data-free quantization, we want to minimize this error in order to achieve the highest possible fidelity to the original model. In the following section, we describe how we can efficiently reduce the quantization error for a fixed target bit-width b .

3.1. Residual Expansion

We propose to quantize the residual errors introduced by the quantization process. Although the proposed method can be applied to any tensor, let's consider a weight tensor W . In the full-precision space (\mathbb{R}), its first approximation is $R^1 = Q^{-1}(Q(W))$. To reduce the quantization error, we define R^2 as the quantized residual error

$$R^2 = Q^{-1}(Q(W - R^1)) \quad (2)$$

Consequently, during the quantized inference, we compute $R^1 X + R^2 X \approx W X$ which provides a finer approximation than the simple evaluation $R^1 X$. The process can be generalized to any expansion order K .

$$R^K = Q^{-1} \left(Q \left(W - \sum_{k=1}^{K-1} R^k \right) \right) \quad (3)$$

The resulting expanded layer is illustrated in Figure 1 (a) in the case $K = 4$. Intuitively, an expansion (R^1, \dots, R^K) provides the approximation $\sum_{k=1}^K R^k$ of W and this approximation converges exponentially fast to the original

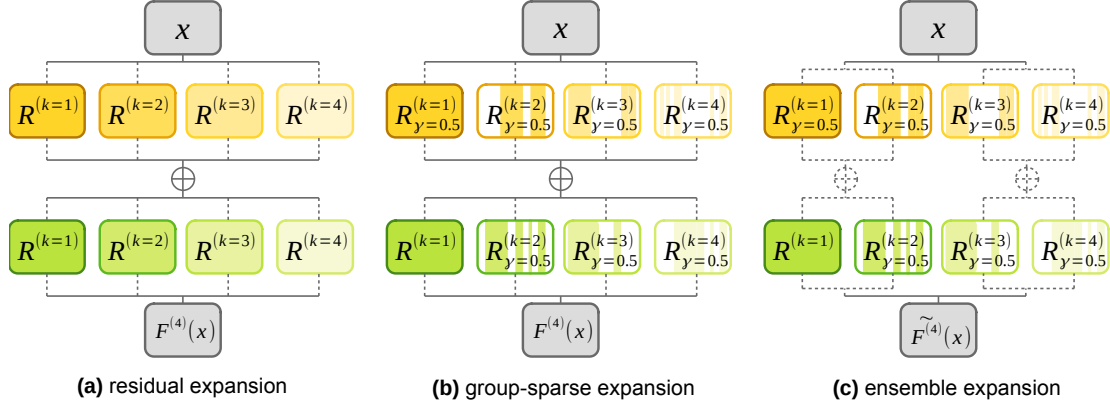


Figure 1: Illustration of the proposed method for a two-layers neural network. (a) residual expansion at order 4: the intensity of the colormap indicates the magnitude of the residual error. (b) group-sparse expansion for orders $k \geq 1$ ($\gamma = 50\%$ sparsity). (c) ensemble expansion with two predictors. Dashed lines indicate parallel computations.

full-precision weights with respect to K . As the support of the quantization error space is smaller than one quantization step, the error decreases by a factor larger than 2^b with each expansion term (more details in Appendix A). Furthermore, as the quantization error decreases, it is expected that the prediction of the quantized model would achieve a closer match to the original predictions. This is especially important in the context of data-free quantization as we, not only, do not have the option to perform fine-tuning in order to recover accuracy but also can not evaluate the degradation of the model on a calibration/validation set. Nonetheless, we can estimate an upper bound on the maximum error ϵ_{\max} introduced by quantization on the predictions as

$$\epsilon_{\max} \leq U = \prod_{l=1}^L \left(\sum_{i=1}^l \left(\frac{1}{2^{b-1} - 1} \right)^{K-1} \frac{s_i}{2} + 1 \right) - 1 \quad (4)$$

The detailed derivations are provided in Appendix B. This implies that, in practice and regardless on the quantization operator, a network can be quantized with high fidelity with only a few expansion orders to fit a given bit-width. However, with this formulation, the overhead computations induced by the expansion is non-negligible. In the following section, we provide a solution to tackle this issue.

3.2. Sparse Expansion

The residual expansion as defined in equation 3 is based upon the assumption that the quantization error is equally important for every neuron. Thus, we propose to reduce the overhead cost by only expanding the most important neurons. However, in data-free compression we do not have access to activations or gradients: hence, we measure the relative importance of a neuron in a layer by the norm of its weights (Molchanov et al., 2016; Yvinec et al., 2022b).

The resulting expanded layer is illustrated in Figure 1 (b). Given a target budget γ (in %) of overhead computations, we only expand the $\frac{\gamma}{K-1}\%$ most important neurons. Similarly to what precedes, each expansion order is derived sequentially from previous orders (see Algorithm 1 in Appendix E.2) and we can bound the quantization error for the sparse expansion (see Appendix A). Also note that in the sparse expansion, we allow higher expansion orders to re-consider neurons that were previously considered unimportant. Consequently, on top of improving the exponential convergence as well as lowering the upper bound on the maximum error with respect to the overhead computations, this method systematically outperforms the standard residual expansion in practice. Proof of this result can be found in Appendix C.

The budget γ of overhead computations can be set so as not to introduce computational overhead, depending on the bit-width b (*i.e.* for a hardware supporting 8 and 1 bit (binary) quantization, we will set a budget $\gamma \leq \frac{8}{1} - 1 = 700\%$ in binary operations). This budget is then split across layers using a simple linear repartition. This strategy gives more emphasis to the layers closest to the prediction head which also correspond to the largest layers, and empirically provides the best results (see Appendix D for a comparison of different budget splitting strategies). As a result, given a number bit operations (BOPS), the expanded model can better fit the inference device while preserving the full-precision accuracy. Furthermore, all the added computations are performed in parallel which reduces their cost in practice. In the following section, we assume that heavy parallelization can be achieved on the target device (*e.g.* CPUs and GPUs) and propose a way to leverage it using an ensemble approximation.

3.3. Ensembling from Expansion

So far (see Figure 1 (a-b)) each layer computes the $R^k \times X$ for all orders k and then sum the results before applying the non-linearity. Intuitively, a better way to leverage parallelization would be to only sum the results after the last layer (Figure 1 (c)), akin to an ensemble model where the elements in the ensemble corresponds to the expansion orders k . To do so, we exploit two assumptions. First, the activation functions σ of the model satisfy the following:

$$\sigma(\cdot + \epsilon) \approx \sigma(\cdot) + \sigma(\epsilon) \quad (5)$$

When $|\epsilon| \rightarrow 0$. This holds true for most popular activation functions such as ReLU, SiLU, GeLU or sigmoid. Second, the exponential convergence of the expansion terms (Equation 4) ensures that the first expansion orders are preponderant w.r.t. the subsequent ones. With this in mind, we can group the expansion orders in M clusters that each contain K_m successive expansion orders (with $m \in [|1, M|]$ and $K_1 + \dots + K_M = K$ the total number of orders in the expansion). For each of these clusters, the sum of the expansion orders that are contained inside must have negligible dynamics with regards to the previous cluster (see Appendix L on how to empirically group expansion orders) to successively apply Equation 5. Finally, we can define the M quantized networks of the ensemble as having the same architecture as the original model F , except that the biases of the model are all assigned to F_1 . For each $m = 1, \dots, M$, the weights of the m^{th} predictor corresponds to the sum over the residuals at orders belonging to the m^{th} cluster.

Proof of this approximation as well as a summary of the ensembling protocol can be found in Appendix E. This ensemble approximation (Figure 1 (c)) also comes with strong theoretical guarantees (see Appendix B) on accuracy preservation depending on expansion order grouping. Furthermore, it allows better usage of the potential parallelization capacities of a target hardware (per-model instead of per-layer parallelization), as will be shown in the upcoming experiments.

4. Quantization Experiments

In the following sections, we first go through the implementation requirements and efficient strategies to fully leverage the proposed expansions. Second, we perform a comparison of each expansion methods in order to show the flexibility of REx with respect to the bit-width. Third, we compare REx to other quantization schemes under the constraint of equal bit operations as well as under the assumption of heavy parallelization for ensembling. Finally, we validate for each expansion their respective upper bound on the maximum error with respect to the original predictions.

4.1. Implementation Details and Benchmarks

We ran our tests on 6 different backbones, including ConvNets and transformers and 4 tasks from both computer vision and natural language processing. We used ImageNet (Deng et al., 2009), Pascal VOC 2012 (Everingham et al., 2012), CityScapes dataset (Cordts et al., 2016) and GLUE (Wang et al., 2018).

Unless stated otherwise, we apply symmetric, static, per-channel quantization as defined in Gholami et al. (2021) and perform batch-normalization folding prior to any processing using the optimal method by Yvinec et al. (2022a). In order to leverage the existing efficient implementations of the convolutional layers and fully-connected layers in CUDA, we propose to implement the expanded layer using a single kernel rather than K kernels. This is achieved by concatenating the kernels along the output dimension. Consequently, the challenge of efficiently split the computations to fully leverage the target device computational power is left to the inference engine. In practice, this results in both better performance and less work in order to adapt the method to existing engines such as OpenVino (Intel, 2022) and TensorRT (Nvidia, 2022). The libraries, pre-trained model checkpoints and datasets information, are detailed in Appendix F. We evaluate the pre-processing time required by REx and compare it to other generic data-free quantization methods in Appendix N. In the following section, we confirm the hinted benefits from each of the proposed expansions.

4.2. Flexible Quantization

Figure 2 shows different trade-offs enabled by REx on different bit-widths for an EfficientNet-B0 on ImageNet. First, the baseline quantization with the baseline quantization operator from Krishnamoorthi (2018) (as depicted by the pentagon of different colors-one for each bit width) offers no trade-off possibility given a specific bit-width and usually performs poorly below int8 quantization (e.g. barely reaching 20.290% top1 accuracy in W6/A6 quantization). REx, however, in the same setup, enables finding several trade-offs for each specific bit-width (e.g. int4 and ternary on Figure 2) and supporting hardware. Furthermore, the sparse expansion enables finding more potential trade-offs (by varying the budget and expansion order) for every bit-width. Those trade-offs are generally more interesting than comparable ones obtained using the base expansion, which empirically confirm the theoretical results in Appendix C. We provide more empirical results in Appendix M to show the stability of these results across several convolutional architectures and bit-widths.

Although we theoretically and empirically demonstrate the benefit of higher sparse order over regular expansion (see Appendix M), we do not require the use of extremely sparse

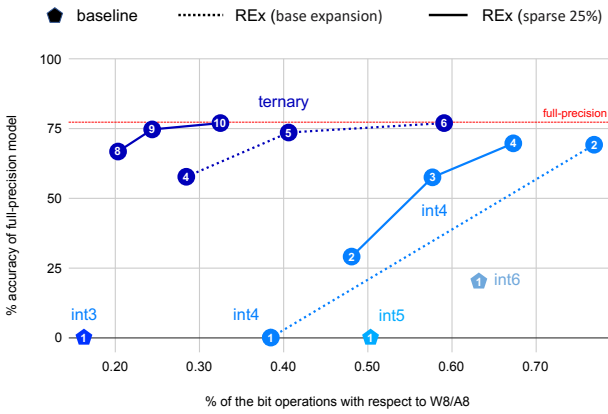


Figure 2: Accuracy *vs.* inference time, for EfficientNet B0. The higher (accuracy) and the further to the left (inference cost) the better. The pentagons show the baseline results with W3/A3, W4/A4, W5/A5 and W6/A6 quantization. The dashed lines show the trade-offs performance of REx in W4/A4 and ternary quantization. Finally, the plain lines show REx (with sparsity) also in W4/A4 and ternary quantization. The numbers in the symbols stands for the expansion order. REx, and *a fortiori* the sparse version, enables better trade-offs.

residues in order to get the best accuracy. For instance in Figure 2 we reach full-precision accuracy using 25% sparse residues. In other words, the process converges fast with respect to the sparsity rates. We provide a more detailed analysis of the sparsity hyper-parameter in Appendix J. All in all, these results demonstrate the flexibility of REx to find good accuracy *v.s.* speed trade-offs, given a budget of total bit operations (BOPs) to fit. In the following section, we evaluate REx ability to outperform existing quantization methods in terms of equal bops as well as in the context of heavy parallelization.

4.3. Main Results

4.3.1. EQUAL BOPs

In order to highlight the benefits of residual quantization errors expansions as a stand alone improvement upon existing methods with equal BOPs, we compare REx using the naive quantization operator from (Krishnamoorthi, 2018) on a variety of reference benchmarks. First, in Table 1, we report the performance on three different computer vision networks between state-of-the-art methods in W6/A6 quantization (other setups are discussed in Appendix G) and REx using a sparse expansion at order $K = 2$ using 50% of a 4 bits representations in order to get a similar total number of bit operations (150% of 4 bits \approx 6 bits). For all networks, REx significantly outperform recent state-of-the-art data-free quantization methods at equal BOPs. Furthermore, we confirm these results on object detection and image segmentation in Appendix G.

Table 1: Comparison at equal BOPs (*i.e.* no-parallelization) with existing methods in W6/A6 and REx with W4/A6 +50% of one 4 bits residue.

DNN	method	year	bits	Acc
ResNet 50	full-precision			76.15
	DFQ	ICCV 2019	6	71.36
	ZeroQ	CVPR 2020	6	72.93
	DSG	CVPR 2021	6	74.07
	GDFQ	ECCV 2020	6	74.59
	SQuant	ICLR 2022	6	75.95
	SPIQ	WACV 2023	6	75.98
MobNet v2	REx	-	150% \times 4	76.01
	full-precision			71.80
	DFQ	ICCV 2019	6	45.84
	SQuant	ICLR 2022	6	61.87
EffNet B0	SPIQ	WACV 2023	6	63.24
	REx	-	150% \times 4	64.20
	full-precision			77.10
DFQ	ICCV 2019	6	43.08	
	SQuant	ICLR 2022	6	54.51
	REx	-	150% \times 4	57.63

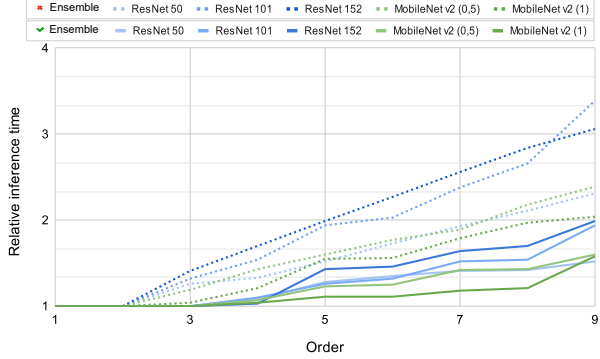


Figure 3: Standardized inference time on ImageNet of different architectures. We demonstrate that parallelization of the overhead computations brought by the proposed ensemble approximation drastically reduces their impact on runtime on a intel m3 CPU.

Second, In Table 2, we perform a similar experiment on NLP using Bert (Devlin et al., 2018). Similarly to our results on ConvNets, REx can find better accuracy per bits trade-offs as compared to the fours references including non-uniform quantization (Miyashita et al., 2016). Furthermore, if we consider parallelization, REx can offer even higher accuracy results using ensemble approximation, as shown in what follows.

4.3.2. LEVERAGING PARALLELIZATION

On large devices using CPUs or GPUs for inference, parallelization of the computations within a layer or a model can drastically reduce the runtime. In Figure 3, we showcase

Table 2: GLUE task quantized in W4/A8. We consider the BERT transformer architecture (Devlin et al., 2018) and provide the original performance (from the article) of BERT on GLUE as well as our reproduced results (reproduced). REx is applied to the weights with 3 bits + 33% sparse expansion.

task	original	reproduced	uniform	log	SQuant	SPIQ	REx
CoLA	49.23	47.90	45.60	45.67	<u>46.88</u>	46.23	47.02
SST-2	91.97	92.32	<u>91.81</u>	91.53	91.09	91.01	91.88
MRPC	89.47/85.29	89.32/85.41	88.24/84.49	86.54/82.69	88.78/85.24	88.78/85.06	88.71/85.12
STS-B	83.95/83.70	84.01/83.87	<u>83.89/83.85</u>	84.01/83.81	83.80/83.65	83.49/83.47	83.92/83.85
QQP	88.40/84.31	90.77/84.65	89.56/83.65	90.30/84.04	<u>90.34/84.32</u>	90.30/84.21	90.50/84.35
MNLI	80.61/81.08	80.54/80.71	<u>78.96/79.13</u>	78.96/79.71	78.35/79.56	<u>78.52/79.86</u>	79.03/79.96
QNLI	87.46	91.47	89.36	89.52	90.08	<u>89.64</u>	90.08
RTE	61.73	61.82	<u>60.96</u>	60.46	60.21	60.21	61.20
WNLI	45.07	43.76	39.06	42.19	42.56	42.12	42.63

the normalized inference times (*i.e.* the ratio between the runtime of the expanded networks and the baseline quantized model) for several ResNets and MobileNets on ImageNet. On the one hand, as indicated by the dashed plots (no ensembling), the relative inference time grows sub-linearly for each network, e.g. order 2 comes at virtually no cost in terms of inference time, while using higher orders may induce a noticeable slow down: < 50% speed reduction for order $K = 3$, and about 100% at order $K = 5$. On the other hand, when we evaluate ensembles, and specifically two predictors with similar sizes (see Appendix L), we observe that we can expand the quantized models up to order 4 without noticeably degrading the inference speed even a small CPU such as the intel m3. This is due to the more efficient parallelization using the proposed ensemble approximation.

Consequently, in Table 3 we compare REx to other data-free quantization methods under this assumption of heavy parallelization (and asymmetric quantization). We consider an ensemble of two weak predictors with each 2 expansion orders: R^1, R^2 for the first predictor and R^3, R^4 for the second. Our results on the challenging MobileNet show that, as compared to the most recent data-free quantization operators that do not use data-generation (no-DG) such as SQuant (Cong et al., 2022) and SPIQ (Yvinec et al., 2023), the proposed REx method improves the accuracy by 16.35 points in 4 bits quantization. Furthermore, data-free techniques that leverage synthetic data are usually known for their higher performance as compared the methods that only focus on the quantization operator. Nonetheless, REx still manages to improve upon recent techniques including IntraQ (Zhong et al., 2022) and AIT (Choi et al., 2022) by 5.26 points in the advantageous and realistic assumption of heavy parallelized inference. These observations can be generalized to more DNN architectures as discussed in Appendix O. We can conclude that REx allows to find better accuracy *v.s.* speed trade-offs given the possibility to leverage parallelization on larger hardware.

Table 3: Accuracy for MobileNet V2 on ImageNet with 8 bits activations. REx uses ensembling of two weak predictors each sharing the same number of bit operations and comparable runtime, based on Figure 3.

method	year	no-DG		accuracy
		full-precision	bits	
				71.80
OCS	ICML 2019	✓	8	71.10
DFQ	ICCV 2019	✓	8	70.92
SQNR	ICML 2019	✓	8	71.2
ZeroQ	CVPR 2020	✗	8	71.61
SPIQ	WACV 2023	✓	8	71.79
GDFQ	ECCV 2020	✗	8	71.80
REx	-	✓	8	71.80
DFQ	ICCV 2019	✓	4	0.10
ZeroQ	CVPR 2020	✗	4	49.83
GDFQ	ECCV 2020	✗	4	51.30
SQuant	ICLR 2022	✓	4	55.38
MixMix	CVPR 2021	✗	4	65.38
AIT	CVPR 2022	✗	4	66.47
IntraQ	CVPR 2022	✗	4	65.10
REx	-	✓	4	71.73

Table 4: Upper bound U (see theorem B.1, B.2 and B.3) over the maximum error as compared to the corresponding empirical measurement $U_{\text{empirical}}$ of that error for a VGG 16 (Simonyan & Zisserman, 2014) trained on ImageNet. The closer the upper bound U to the value $U_{\text{empirical}}$ the better.

bits	K	sparsity	ensemble	U	$U_{\text{empirical}}$
8	1	✗	✗	0.12	0.05
8	4	✗	✗	1.99×10^{-7}	1.78×10^{-7}
8	2	50%	✗	0.06	0.05
8	4	50%	✗	1.17×10^{-7}	0.65×10^{-7}
8	2	✗	✓	0.09	0.02
8	4	✗	✓	0.47×10^{-4}	0.43×10^{-4}

Table 5: We report the different trade-offs achieved with REx expanding over different proposed quantization operators in int4 as compared to their performance in int8.

method	W4	W4 + 25%	W4 + 50%	W4 + 75%	W8
naive	0.1	53.11	64.20	71.61	70.92
SQuant	4.23	58.64	67.43	71.74	71.68
SPIQ	5.81	59.37	68.82	71.79	71.79
AdaR	6.17	60.30	69.80	71.77	71.75
BrecQ	66.57	70.94	71.28	71.76	71.76

4.4. Empirical Validation of the Theoretical Bounds

In Table 4, we validate the proposed upper bound U on the maximum error on the predictions (see Equation 4) on a VGG-16 (Simonyan & Zisserman, 2014) trained on ImageNet. The tightness of the provided theoretical results can be estimated from the gap between our estimation and the empirical maximum error $U_{\text{empirical}}$ from quantization on the predictions, which is measured as the infinite norm between the full-precision and quantized logits. We observe that a naïve 8-bits quantization (*i.e.* no expansion) leads to an upper bound $U = 0.12$, while we observe $U_{\text{empirical}} = 0.05$. The norms of the logits is equal to 0.3423. Therefore, the proposed upper bound is relatively tight and significantly lower than the logits magnitude: in such a case, due to overconfidence, the error shouldn't affect the classification. The proposed upper bound is even tighter for larger values of K , and becomes lower and lower (for both the theoretical and corresponding empirical maximum errors) when introducing sparsity. Last but not least, we see on the last two rows in Table 4 that U stays tight when using the ensemble approximation. This further demonstrates the good properties of the proposed expansion, sparse expansion and ensemble approximation in REx in addition to the relevance of its theoretical guarantees, which are critical in data-free quantization.

4.5. Flexibility with respect to the Quantization Operator

Most recent approaches for data-free quantization focus on designing better quantization operators. Interestingly, our approach is agnostic to the choice of the quantization operator and can thus be combined with these approaches without bells and whistles. In Table 5, we report the possible trade-offs achievable with REx combined with recent approaches focusing on the quantization operator. First, when used with SQuant (Cong et al., 2022), REx achieves impressive accuracy in W4, even outperforming W8 quantization. SPIQ (Yvinec et al., 2023), can also be adapted with REx in order to achieve good accuracy using only 4 bits representation as it benefits from finer weight quantization. This explains the slightly higher accuracies than SQuant

using 25% and 50% sparsity. Finally, with AdaRound (Nagel et al., 2020) and BrecQ (Li et al., 2021a), two PTQ techniques, we observe similar results as expected. In particular, BrecQ which already achieves decent accuracy in W4/4 with a 5.23 points accuracy drop gets closer to the original accuracy (0.86 point accuracy drop) using a quarter of the expansion. Those results demonstrate REx versatility.

5. Conclusion

In this work, we proposed to use the expansion of residual quantization errors, as novel data-free quantization method, dubbed REx. In order to find the best accuracy *v.s.* speed trade-offs, we improved upon the base residual expansion with group-sparsity and ensemble approximation. The resulting quantization method is flexible with respect to both hardware bit-width support as well as parallelization capacities. We demonstrated the exponential convergence of the quantized weights obtained through the different expansion method towards the full-precision model. Furthermore, we showed the validity of the ensemble approximation derived from the proposed expansion. These theoretical guarantees are crucial in the context of data-free quantization where we cannot empirically measure the accuracy degradation in an industrial application context. In addition to our theoretical finding, we showed the added value of the proposed REx method through extensive empirical validation. As such, REx significantly outperforms recent data-free quantization methods on a wide range of ConvNet architectures applied to ImageNet classification, Pascal VOC object detection, CityScapes semantic segmentation as well as transformers on GLUE text classification. Last but not least, the ideas presented in this paper are orthogonal to most recent approaches focusing on improving the quantization operator, and hence can straightforwardly be combined with those approaches.

5.1. Limitations:

The residual expansion method introduced in this paper does not adapt to the inter-layer importance and runtime cost discrepancies. An interesting future work would thus consist in applying more expansion orders on the most important layers *w.r.t.* the model accuracy, as well as using fewer orders for the most computationally expensive layers.

References

Achterhold, J., Koehler, J. M., Schmeink, A., and Gennwein, T. Variational network quantization. In *ICLR*, 2018.

Breiman, L. Bagging predictors. *Machine learning*, 24(2):

123–140, 1996.

Breiman, L. Arcing the edge. Technical report, Technical Report 486, Statistics Department, University of California at ..., 1997.

Cai, Y., Yao, Z., Dong, Z., Gholami, A., Mahoney, M. W., and Keutzer, K. Zeroq: A novel zero shot quantization framework. In *CVPR*, pp. 13169–13178, 2020.

Chen, L.-C., Papandreou, G., Schroff, F., and Adam, H. Rethinking atrous convolution for semantic image segmentation. *arXiv preprint arXiv:1706.05587*, 2017.

Chen, L.-C., Zhu, Y., Papandreou, G., Schroff, F., and Adam, H. Encoder-decoder with atrous separable convolution for semantic image segmentation. In *ECCV*, pp. 801–818, 2018.

Chen, W., Wilson, J., et al. Compressing neural networks with the hashing trick. In *ICML*, pp. 2285–2294, 2015.

Choi, K., Lee, H. Y., Hong, D., Yu, J., Park, N., Kim, Y., and Lee, J. It’s all in the teacher: Zero-shot quantization brought closer to the teacher. In *CVPR*, pp. 8311–8321, 2022.

Cong, G. et al. Squant: On-the-fly data-free quantization via diagonal hessian approximation. *ICLR*, 2022.

Cordts, M., Omran, M., Ramos, S., Rehfeld, T., Enzweiler, M., Benenson, R., Franke, U., Roth, S., and Schiele, B. The cityscapes dataset for semantic urban scene understanding. In *CVPR*, pp. 3213–3223, 2016.

Courbariaux, M., Hubara, I., et al. Binarized neural networks: Training deep neural networks with weights and activations constrained to +1 or -1. *NeurIPS*, 2016.

Deng, J., Dong, W., et al. ImageNet: A Large-Scale Hierarchical Image Database. In *CVPR*, 2009.

Devlin, J., Chang, M.-W., Lee, K., and Toutanova, K. Bert: Pre-training of deep bidirectional transformers for language understanding. *arXiv preprint arXiv:1810.04805*, 2018.

Dietterich, T. G. Ensemble methods in machine learning. In *International workshop on multiple classifier systems*, pp. 1–15. Springer, 2000.

Everingham, M., Van Gool, L., Williams, C. K. I., Winn, J., and Zisserman, A. The PASCAL Visual Object Classes Challenge 2012 (VOC2012) Results. <http://www.pascal-network.org/challenges/VOC/voc2012/workshop/index.html>, 2012.

Feng, B., Wang, Y., Geng, T., Li, A., and Ding, Y. Apnn-tc: Accelerating arbitrary precision neural networks on ampere gpu tensor cores. In *Proceedings of the International Conference for High Performance Computing, Networking, Storage and Analysis*, pp. 1–13, 2021.

Friedman, J., Hastie, T., and Tibshirani, R. Additive logistic regression: a statistical view of boosting (with discussion and a rejoinder by the authors). *The annals of statistics*, 28(2):337–407, 2000.

Gholami, A., Kim, S., Dong, Z., Yao, Z., Mahoney, M. W., and Keutzer, K. A survey of quantization methods for efficient neural network inference. *arXiv preprint arXiv:2103.13630*, 2021.

Gong, Y., Liu, L., Yang, M., and Bourdev, L. Compressing deep convolutional networks using vector quantization. *arXiv preprint arXiv:1412.6115*, 2014.

Han, S., Mao, H., and Dally, W. J. Deep compression: Compressing deep neural networks with pruning, trained quantization and huffman coding. *ICLR*, 2016.

He, K., Zhang, X., et al. Deep residual learning for image recognition. In *CVPR*, pp. 770–778, 2016.

Intel. Intel® distribution of openvino™ toolkit. *Intel*, 2022. URL [Available:https://www.intel.com/content/www/us/en/developer/tools/openvino-toolkit/overview.html](https://www.intel.com/content/www/us/en/developer/tools/openvino-toolkit/overview.html).

Jacob, B., Kligys, S., Chen, B., Zhu, M., Tang, M., Howard, A., Adam, H., and Kalenichenko, D. Quantization and training of neural networks for efficient integer-arithmetic-only inference. In *CVPR*, pp. 2704–2713, 2018.

Klarreich, E. Multiplication hits the speed limit. *Communications of the ACM*, 63(1):11–13, 2019.

Krishnamoorthi, R. Quantizing deep convolutional networks for efficient inference: A whitepaper. *arXiv preprint arXiv:1806.08342*, 2018.

Li, Y., Gong, R., Tan, X., Yang, Y., Hu, P., Zhang, Q., Yu, F., Wang, W., and Gu, S. Brecq: Pushing the limit of post-training quantization by block reconstruction. *NeurIPS*, 2021a.

Li, Y., Zhu, F., Gong, R., Shen, M., Dong, X., Yu, F., Lu, S., and Gu, S. Mixmix: All you need for data-free compression are feature and data mixing. In *ICCV*, pp. 4410–4419, 2021b.

Lin, D., Talathi, S., and Annapureddy, S. Fixed point quantization of deep convolutional networks. In *ICML*, pp. 2849–2858. PMLR, 2016.

Liu, W., Anguelov, D., Erhan, D., Szegedy, C., Reed, S., Fu, C.-Y., and Berg, A. C. Ssd: Single shot multibox detector. In *ECCV*, pp. 21–37. Springer, 2016.

Louizos, C., Reisser, M., Blankevoort, T., Gavves, E., and Welling, M. Relaxed quantization for discretized neural networks. *ICLR*, 2018.

Mallat, S. G. A theory for multiresolution signal decomposition: the wavelet representation. In *Fundamental Papers in Wavelet Theory*, pp. 494–513. Princeton University Press, 2009.

Meller, E., Finkelstein, A., Almog, U., and Grobman, M. Same, same but different: Recovering neural network quantization error through weight factorization. In *ICML*, pp. 4486–4495, 2019.

Miyashita, D., Lee, E. H., and Murmann, B. Convolutional neural networks using logarithmic data representation. *arXiv preprint arXiv:1603.01025*, 2016.

Molchanov, P., Tyree, S., Karras, T., Aila, T., and Kautz, J. Pruning convolutional neural networks for resource efficient inference. *arXiv preprint arXiv:1611.06440*, 2016.

Nagel, M., Baalen, M. v., et al. Data-free quantization through weight equalization and bias correction. In *ICCV*, pp. 1325–1334, 2019.

Nagel, M., Amjad, R. A., Van Baalen, M., Louizos, C., and Blankevoort, T. Up or down? adaptive rounding for post-training quantization. In *ICML*, pp. 7197–7206. PMLR, 2020.

Nvidia. Nvidia a100 tensor core gpu architecture. web tech report (<https://images.nvidia.com/aem-dam/en-zz/Solutions/data-center/nvidia-ampere-architecture-whitepaper.pdf>), 2021.

Nvidia. Nvidia distribution of tensorrt toolkit. *Nvidia*, 2022. URL Available: <https://developer.nvidia.com/tensorrt>.

Oh, S., Sim, H., Lee, S., and Lee, J. Automated log-scale quantization for low-cost deep neural networks. In *CVPR*, pp. 742–751, 2021.

Rabbani, M. Jpeg2000: Image compression fundamentals, standards and practice. *Journal of Electronic Imaging*, 11(2):286, 2002.

Robinson, C. Untether.ai boqueria 1458 risc-v core ai accelerator, Aug 2022. URL <https://www.servethehome.com/untether-ai-boqueria-1458-risc-v-core-ai-accelerator-hc34/>.

Sandler, M., Howard, A., et al. Mobilenetv2: Inverted residuals and linear bottlenecks. In *CVPR*, pp. 4510–4520, 2018.

Sheng, T., Feng, C., Zhuo, S., Zhang, X., Shen, L., and Aleksic, M. A quantization-friendly separable convolution for mobilenets. In *2018 1st Workshop on Energy Efficient Machine Learning and Cognitive Computing for Embedded Applications (EMC2)*, pp. 14–18. IEEE, 2018.

Simonyan, K. and Zisserman, A. Very deep convolutional networks for large-scale image recognition. *BMVC 2014*, 2014.

Stock, P., Graham, B., Gribonval, R., and Jégou, H. Equi-normalization of neural networks. *ICLR*, 2019.

Ullrich, K., Meeds, E., and Welling, M. Soft weight-sharing for neural network compression. *ICLR*, 2017.

Wang, A., Singh, A., Michael, J., Hill, F., Levy, O., and Bowman, S. GLUE: A multi-task benchmark and analysis platform for natural language understanding. In *Proceedings of the 2018 EMNLP Workshop BlackboxNLP: Analyzing and Interpreting Neural Networks for NLP*, pp. 353–355, Brussels, Belgium, November 2018. Association for Computational Linguistics. doi: 10.18653/v1/W18-5446. URL <https://aclanthology.org/W18-5446>.

Wu, S., Li, G., Chen, F., and Shi, L. Training and inference with integers in deep neural networks. *ICLR*, 2018.

Xu, S., Li, H., Zhuang, B., Liu, J., Cao, J., Liang, C., and Tan, M. Generative low-bitwidth data free quantization. In *ECCV*, pp. 1–17. Springer, 2020.

Yvinec, E., Dapogny, A., and Bailly, K. To fold or not to fold: a necessary and sufficient condition on batch-normalization layers folding. *IJCAI*, 2022a.

Yvinec, E., Dapogny, A., Cord, M., and Bailly, K. SInGE: Sparsity via integrated gradients estimation of neuron relevance. In Oh, A. H., Agarwal, A., Belgrave, D., and Cho, K. (eds.), *NeurIPS*, 2022b. URL https://openreview.net/forum?id=oQIJsMlyaW_.

Yvinec, E., Dapogny, A., Cord, M., and Bailly, K. Spiq: Data-free per-channel static input quantization. *WACV*, 2023.

Zhang, X., Qin, H., Ding, Y., Gong, R., Yan, Q., Tao, R., Li, Y., Yu, F., and Liu, X. Diversifying sample generation for accurate data-free quantization. In *CVPR*, pp. 15658–15667, 2021.

Zhang, Y., Zhang, Z., and Lew, L. Pokebnn: A binary pursuit of lightweight accuracy. In *Proceedings of the IEEE/CVF Conference on Computer Vision and Pattern Recognition*, pp. 12475–12485, 2022.

Zhao, R., Hu, Y., Dotzel, J., De Sa, C., and Zhang, Z. Improving neural network quantization without retraining using outlier channel splitting. In *ICML*, pp. 7543–7552, 2019.

Zhong, Y., Lin, M., Nan, G., Liu, J., Zhang, B., Tian, Y., and Ji, R. Intraq: Learning synthetic images with intra-class heterogeneity for zero-shot network quantization. In *CVPR*, pp. 12339–12348, 2022.

Zhou, A., Yao, A., Guo, Y., Xu, L., and Chen, Y. Incremental network quantization: Towards lossless cnns with low-precision weights. *ICLR*, 2017.

Zhou, S., Wu, Y., Ni, Z., Zhou, X., Wen, H., and Zou, Y. Dorefa-net: Training low bitwidth convolutional neural networks with low bitwidth gradients. *arXiv preprint arXiv:1606.06160*, 2016.

Zhu, S., Dong, X., and Su, H. Binary ensemble neural network: More bits per network or more networks per bit? In *CVPR*, pp. 4923–4932, 2019.

Contents

Exponential Convergence	12
Upper Bound Error	14
Sparse Expansion Outperforms Standard Expansion	17
Sparse Budget Split Across Layers	18
Ensembling Protocol	18
Implementation Details and Datasets	20
Other Results on ConvNets	21
Operation Head-count	22
Developments and Binary Representation	22
On the limit value of K	23
The Robustness to the Value of γ	24
How to set predictors size	24
Detailed Trade-Offs of the Expansions	26
Pre-Processing Time	27
More Parallelization Results	28

A. Exponential Convergence

The exponential convergence can be proved for the three methods: expansion, sparse expansion and expansion ensembling. We first prove it for the expansion on sequential models, then generalize the result to more diverse architectures and finally prove the result for the sparse expansion and ensembling. Before detailing the proof of lemma A.1, we empirically motivate the assumption of symmetry over the weigh values distribution. In Figure 4, we plot the distributions of the weights of several layers of a ResNet 50 trained on ImageNet. The assumption is often satisfied in practice. Furthermore, in any instances where it would not be satisfied, it can be enforced using asymmetric quantization.

Lemma A.1. *Let f be a layer with weights $W \in \mathbb{R}^n$ with a symmetric distribution. We denote $R^{(k)}$ the k^{th} quantized weight from the corresponding residual error. Then the error between the rescaled $W^{(K)} = Q^{-1}(R^{(K)})$ and original weights W decreases exponentially, i.e.:*

$$\left| w - \sum_{k=1}^K w^{(k)} \right| \leq \left(\frac{1}{2^{b-1} - 1} \right)^{K-1} \frac{(\lambda_{R^{(K)}})_i}{2} \quad (6)$$

where w and $w^{(k)}$ denote the elements of W and $W^{(k)}$ and $(\lambda_{R^{(k)}})_i$ denotes the row-wise rescaling factor at order k corresponding to w , as defined in equation 1.

We work on expanded layers which compute

$$f^{(K)} : x \mapsto \sigma \left(\sum_{k=1}^K R^{(k)} Q(x) \lambda_{R^{(k)}} \lambda_x + b \right) \quad (7)$$

Proof. Assume $K = 1$, then $W^{(1)}$ is the result of the composition of inverse quantization operator and quantization operator, i.e. $W^{(1)} = \lambda \lfloor \frac{W}{\lambda} \rfloor$. By definition of the rounding operator we know that $||a| - a| \leq 0.5$. Thus we have $|w - w^{(1)}| \leq \lambda/2$. Now in the case $k = 2$, we have by definition of the quantization of the residual error and the property of the rounding operator

$$\left| \left\lfloor \frac{w - w^{(1)}}{\lambda^{(2)}} \right\rfloor - \frac{w - w^{(1)}}{\lambda^{(2)}} \right| \leq \frac{1}{2} \quad (8)$$

where $\lambda^{(2)}$ is the rescaling factor in the second order residual R^2 computed from $w - w^{(1)}$. The quantized weights are thus given by:

$$\left| w - \sum_{i=1}^2 w^{(i)} \right| \leq \frac{\lambda^{(2)}}{2} \quad (9)$$

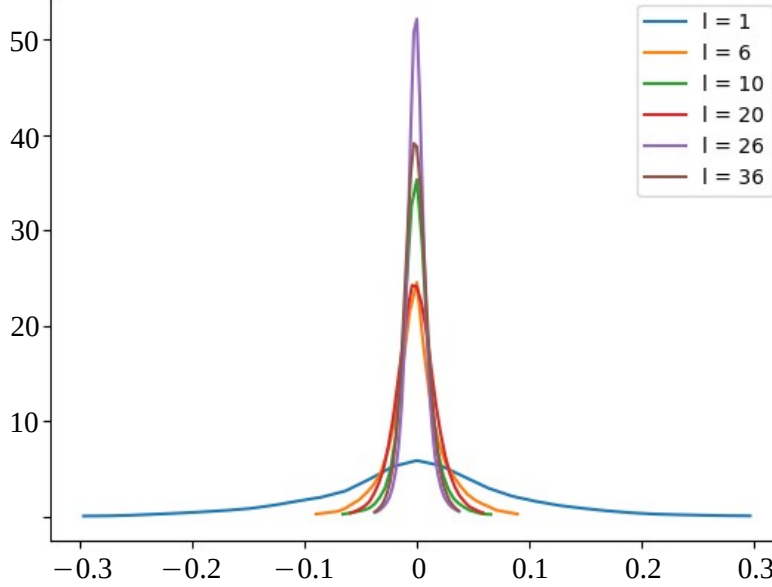


Figure 4: Distribution of the scalar weight values of different layers of a ResNet 50 trained on ImageNet. We observe that every distribution is symmetric around 0.

Because the weight distribution is symmetric we know that for any k , $\lambda^{(K)} = \frac{\max\{w - \sum_{k=1}^{K-1} w^{(k)}\}}{2^{b-1}-1}$. Also, by definition we have $\max\{w - \sum_{k=1}^{K-1} w^{(k)}\} \leq \lambda^{(K-1)}$. Thus:

$$\left| w - \sum_{k=1}^2 w^{(k)} \right| \leq \left(\frac{1}{2^{b-1}-1} \right) \frac{\lambda}{2} \quad (10)$$

We conclude by using a trivial induction proof. \square

As an immediate consequence we have the following corollary which justifies the expansion appellation:

Corollary A.2. *Let f be a layer of real-valued weights W with a symmetric distribution and $R^{(k)}$ the k^{th} quantized weight from the corresponding residual error. Then,*

$$\mathbb{E} \left[\left\| f - \sum_{k=1}^K f^{(k)} \right\| \right] \geq \mathbb{E} \left[\left\| f - \sum_{k=1}^{K+1} f^{(k)} \right\| \right] \quad (11)$$

and $f = \sum_{k=1}^{\infty} f^{(k)}$.

The first inequality results from detailing the induction in the previous proof. Instead of an upper bound on the error over all the scalar values we consider each error and show using the same properties that they go down after each step. $f = \sum_{k=1}^{\infty} f^{(k)}$ is a direct consequence of equation 6.

This result can be extended to more sophisticated architectures. To do so we simply need to address specific attributes such as skip connections, concatenations and other activation functions.

Skip Connections and Concatenations In the case of skip connections, the graph is split from a starting layer l_1 and split in at least two branches that are added after layer l_2 and l_3 . Assuming we can compute the upper bound for each branch (sub-networks) we simply add these sub-errors. In the case of U-nets, where skip connections contain skip connections, we simply perform this process recursively.

A similar approach can be applied to address concatenations. However in this case we keep the largest value instead of adding them.

Other Activation Functions Although ReLU activations are predominant in modern DNNs, there are still many other widely used activation functions such as SiLU, GeLU or even sigmoid. SiLU and GeLU are bounded by the ReLU on the positive side which is where the highest errors occur. Consequently, the upperbound is invariant to GeLU and SiLU activation functions (although under more assumptions on the support, the upper bound could be tightened for ReLU and should be modified for GeLU and SiLU). On the other hand, for sigmoid activations or similar activations (e.g. tanh), the upper bound becomes an upper bound on X in the domain of F instead of X on the unit circle.

Sparse Expansion Let $N_i^{(k)}$ denotes the L_1 norm of an output channel i of the k -th order residue $R^{(k)}$. The sparse residue is defined as:

$$\left(R_\gamma^{(k)} \right)_i = (R^{(k)})_i \cdot \mathbb{1}_\gamma^{(k)} \quad (12)$$

where \cdot is the element-wise multiplication, $\mathbb{1}_\gamma^{(k)} = \mathbb{1}_{\{N_i^{(k)} \geq \tau_\gamma^{(k)}\}}$ and $\tau_\gamma^{(k)}$ is a threshold defined as the γ percentile of $N^{(k)}$. In other words, we remove a proportion γ of channels from residue $R^{(k)}$ that are the least important, as indicated by their norm $N^{(k)}$. Note however that these pruned channels can be encoded in subsequent residuals, *i.e.* $R^{(k')}$, with $k' > k$. The result from Lemma A.1 becomes:

Lemma A.3. *Let f be a layer of real-valued weights W with a symmetric distribution. Then we have*

$$\begin{aligned} & \left| w - \left(\sum_{k=1}^{K-1} w^{(k)} + Q^{-1} \left(R_\gamma^{(K)} \right) \right) \right| \\ & \leq \frac{\|N^{(K)} \cdot \mathbb{1}_\gamma^{(K)}\|_\infty (\lambda_{R^{(k)}})_i}{(2^{b-1} - 1)^K 2} \end{aligned} \quad (13)$$

where $\|\cdot\|_\infty$ is the infinite norm operator with the convention that $\|0\|_\infty = 1$ and $(\lambda_{R^{(k)}})_i$ denotes the row-wise rescaling factor at order K corresponding to w .

Proof. From equation 6, we have:

$$\left| w - \left(\sum_{k=1}^{K-1} w^{(k)} + Q^{-1} \left(R_1^{(K)} \right) \right) \right| \leq \frac{(\lambda_{R^{(K)}})_i}{2} \left(\frac{1}{2^{b-1} - 1} \right)^K \quad (14)$$

which corresponds to the case where $\gamma^l = 1$. If $\gamma^l < 1$, we have two possibilities for w . First, the coordinate in $N^{(K)}$ associated to is greater than $\tau_{\gamma^l}^{(K)}$ then we fall in the case where $R_\gamma^{(K)} = R^{(K)}$ and as such we have the result from equation 6 which is stronger than equation 13. Second, the coordinate in $N^{(K)}$ associated to is lower than $\tau_{\gamma^l}^{(K)}$. Then we have that the difference between the baseline weight w and the slim expansion is bounded by the expansion of lower order and the maximum of the norm $N^{(K)}$ which leads to the result in equation 13. \square

Empirical validation: In lemma A.1 and A.3 we stated the exponential convergence to 0 of the approximation error on the weight values. In order to empirically confirm this theoretical result, we quantize a ResNet 50 trained on ImageNet in ternary values for different orders K . As can be seen in Figure 5, the average error per layer, exponentially converges to 0 which matches our expectations. The figure also confirms the empirical result on the strategies for γ . The higher errors are located on the last layers, thus these layers require more attention.

B. Upper Bound Error

Theorem B.1. *Let F be a trained L layers sequential DNN with ReLU activation $\sigma_{L-1} = \dots = \sigma_1$. We note s_l the largest singular value of W_l , *i.e.* the spectral norm of W_l . Then we have*

$$\begin{aligned} \max_{\|X\|=1} \|F(X) - F(X)^{(K)}\|_\infty & \leq U_{res} \\ U_{res} & = \prod_{l=1}^L \left(\sum_{i=1}^l s_i u_i^{(K)} + 1 \right) - 1 \end{aligned} \quad (15)$$

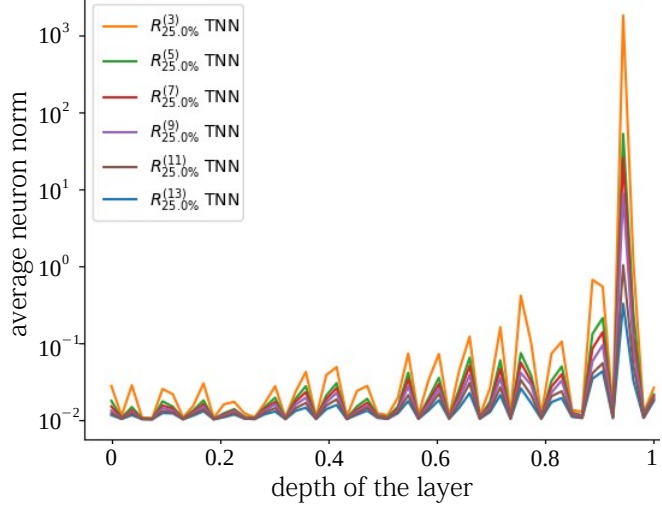


Figure 5: Comparison of the average norm of the quantization error for each layers of a ResNet 50 trained on ImageNet. We observe the exponential convergence stated in lemma A.1 and A.3.

where $u_l^{(K)} = \left(\frac{1}{2^{b-1}-1}\right)^{K-1} \frac{(\lambda_{R^{(K)}})_i}{2}$ from equation 6.

Proof. Let's consider $L = 2$, and $F : X \mapsto B\sigma(Ax)$. For any X in the domain of F such that $\|X\| = 1$, we have

$$\|F(X)\|_2 \leq s_B + s_A + s_B s_A \quad (16)$$

where s_B is the largest singular value of B and s_A is the largest singular value of A . Following the definition of the 2-norm and ∞ -norm, we get that

$$s_{A-A^{(K)}} \leq s_A u_A^{(K)} \quad (17)$$

where $s_{A-A^{(K)}}$ is the largest singular value of the residual error of order K , $A - A^{(K)}$ and $u_A^{(K)}$ is derived from equation 6. Consequently, we get

$$\|F(X) - F^{(K)}(X)\|_2 \leq s_B u_B^{(K)} + s_A u_A^{(K)} + s_B u_B^{(K)} s_A u_A^{(K)} \quad (18)$$

□

Sparse Expansion

Theorem B.2. Let F be a trained L layers sequential DNN with ReLU activation $\sigma_{L-1} = \dots = \sigma_1$. We note s_l the largest singular value of W_l , i.e. the spectral norm of W_l . Then we have

$$\begin{aligned} \max_{\|X\|=1} \|F(X) - F(X)^{(K)}\|_{\infty} &\leq U_{\text{sparse}} \\ U_{\text{sparse}} &= \prod_{l=1}^L \left(\sum_{i=1}^l s_i u_i^{(K)} + 1 \right) - 1 \end{aligned} \quad (19)$$

where $u_l^{(K)} = \frac{\|N^{(K)} \cdot \mathbb{1}_\gamma^{(K)}\|_{\infty} (\lambda_{R^{(k)}})_i}{(2^{b-1}-1)^K 2}$ from equation 13.

This results is directly derived from Theorem B.1.

Ensemble Expansion

Theorem B.3. Let F be a L layers feed-forward DNN with ReLU activation $\sigma_{L-1} = \dots = \sigma_1$. The expected error $\mathbb{E} [\|F^{(K)} - \tilde{F}^{(K)}\|]$ due to the ensemble expansion of order K with M predictors, is bounded by U_{ens} which can be approximated as:

$$U_{\text{ens}} \approx \frac{\sum_{k=1}^{K_1} \|R_L^{(k)}\|}{2^{L-1}} \left(1 + \sum_{m=2}^M \prod_{l=1}^{L-1} \sum_{k=K_m}^{K_{m+1}} \|R_L^{(k)}\| \lambda_{\tilde{h}_l^{(k)}} \right) \quad (20)$$

The upper bound U_{ens} is directly deduced from the largest eigenvalues and reduces as the size of the expansion diminishes. Moreover the larger K_1 the faster the convergence which is intuitive as in our approximation $\sigma(x + \epsilon) \approx \sigma(x) + \sigma(\epsilon)$ relies on the fact that $x \gg \epsilon$. Thus the ensembling approximation is a way to find new trade-offs in terms of accuracy and parallelization of the inference. To sum it up, any deep neural network can be approximated by an ensemble expansion of quantized networks, with theoretical guarantees of the approximation error. In practice, as we will showcase in the experiments, this ensemble approximation from expansion of residual errors leads to superior performances in term of accuracy-inference time trade-off. We provide the following intermediate result regarding two-layers DNNs.

Lemma B.4. Let f be a two layers feed-forward DNN with activation function $\sigma = \text{ReLU}$. The expected error $\mathbb{E} [\|f^{(K)} - \tilde{f}^{(K)}\|]$ due to the ensemble expansion of order K is bounded by U defined as:

$$U = \sum_{k=1}^K \left(1 - \mathbb{P} \left(f_1^{(K)} > 0 \cup \tilde{f}_{1,1}^{(K)} > 0 \right) \right) \lambda_{\tilde{f}_{1,2}^{(K)}} \lambda_{R_2^{(k)}} \|R_2^{(k)}\| \times \mathbb{E} [\|\tilde{f}_{1,2}^{(K)}\|] \quad (21)$$

where $\|W\|$, for any set of weights W , denotes the norm operator or equivalently the spectral norm.

Proof. By definition of the ReLU activation function, if we have $f_1^{(K)} > 0$ then the activation function of f_1 behaves as the identity function. Similarly, if $\tilde{f}_{1,1}^{(K)} > 0$ then the activation function of \tilde{f}_1 also behaves as the identity. Therefore, if we have $(f_1^{(K)} > 0) \cup (\tilde{f}_{1,1}^{(K)} > 0)$, then $\tilde{f}_1^{(K)} = f_1^{(K)}$. We deduce that $\mathbb{E} [\|f^{(K)} - \tilde{f}^{(K)}\|]$ is equal to

$$\int_{\{f_1^{(K)} > 0 \cup \tilde{f}_{1,1}^{(K)} > 0\}^C} \|f^{(K)}(x) - \tilde{f}^{(K)}(x)\| \mathbb{P} dx \quad (22)$$

where A^C the complementary set of a set A and x is the input. In the set defined by $\tilde{f}_{1,1}^{(K)}(x) = 0$, the value of $\tilde{f}_1^{(K)}(x)$ is the value of $\tilde{f}_{1,2}^{(K)}(x)$. If we also have $f_1^{(K)}(x) = 0$ then $\|f^{(K)}(x) - \tilde{f}^{(K)}(x)\| = \|\tilde{f}_{1,2}^{(K)}(x)\|$. We can deduce

$$\mathbb{E} [\|f_1^{(K)} - \tilde{f}_1^{(K)}\|] = \left(1 - \mathbb{P} \left(f_1^{(K)} > 0 \cup \tilde{f}_{1,1}^{(K)} > 0 \right) \right) \times \mathbb{E} [\|\tilde{f}_{1,2}^{(K)}\|] \quad (23)$$

The final result comes from the definition of the norm operator of a matrix and equation 32. \square

An immediate limit to lemma B.4 is the difficulty to compute $1 - \mathbb{P} \left(f_1^{(K)} > 0 \cup \tilde{f}_{1,1}^{(K)} > 0 \right)$. However this value can be approached under the assumption that the distribution of the activations is symmetrical around 0. Such instances appear with batch normalization layers and result in $1 - \mathbb{P} \left(f_1^{(K)} > 0 \cup \tilde{f}_{1,1}^{(K)} > 0 \right) \approx \frac{1}{2}$. We also propose to compute the operator norm instead of $\mathbb{E} [\|\tilde{f}_{1,2}^{(K)}\|]$ in order to remain data-free. In consequence, we derive the following corollary.

Corollary B.5. The previous upper bound U on the expected error due to the ensemble expansion can be approximated as follows

$$U \approx \frac{1}{2} \sum_{k=1}^K \|R_2^{(k)}\| \lambda_{\tilde{f}_{1,2}^{(K)}} \lambda_{R_2^{(k)}} \sum_{k=K_1}^K \|R_1^{(k)}\| \lambda_x \lambda_{R_1^{(k)}} \quad (24)$$

In practice, for expansion in b bits, with high values of b (e.g. $b \geq 4$), the single operator $R^{(1)}$ is enough to satisfy equation 31 and $K_1 = 1$. For lower values of b (e.g. ternary quantization), the suitable value for K_1 depends on the DNN architecture, usually ranging from 3 to 6.

Ensembling with more Layers We generalize this result to any feed-forward neural network f with $L > 2$ layers and activation functions $\sigma_1, \dots, \sigma_{L-1}$. Equation 7 becomes:

$$f_L^{(K)}(X_{f_{L-1}^{(K)}}) = \sum_{k=1}^K R_L^{(k)} X_{f_{L-1}^{(K)}} \lambda_{R_L^{(k)}} \lambda_{X_{f_{L-1}^{(K)}}} + b_L \quad (25)$$

where $X_{f_{L-1}^{(K)}} = f_{L-1}^{(K)} \circ \dots \circ f_1^{(K)}(x)$. We reason by induction on the layer $L - 1$. Similarly to what precedes, we assume that we have $\tilde{g}_{L-2}^{(K)}, \dots, \tilde{g}_1^{(K)}$ and $\tilde{h}_{L-2}^{(K)}, \dots, \tilde{h}_1^{(K)}$ such that:

$$f_{L-2}^{(K)} \circ \dots \circ f_1^{(K)}(x) \approx \tilde{g}_{L-2}^{(K)} \circ \dots \circ \tilde{g}_1^{(K)}(x) + \tilde{h}_{L-2}^{(K)} \circ \dots \circ \tilde{h}_1^{(K)}(x) \quad (26)$$

In order to simplify the composition notations, we note X_f the input of a function f . With this in mind Eq. 32 becomes:

$$\begin{cases} \tilde{f}^{(K)}(x) & \approx \sum_{k=1}^K R_L^{(k)} \tilde{f}_{L-1}^{(K)}(x) \lambda_{R_L^{(k)}} \lambda_{\tilde{f}_{L-1}^{(K)}} + b_L \\ \tilde{f}_{L-1}^{(K)}(x) & = \tilde{g}_{L-1}^{(K)}(X_{\tilde{g}_{L-1}^{(K)}}) + \tilde{h}_{L-1}^{(K)}(X_{\tilde{h}_{L-1}^{(K)}}) \\ \tilde{g}_{L-1}^{(K)}(X_{\tilde{g}_{L-1}^{(K)}}) & = \sigma_{L-1} \left(\sum_{k=1}^{K_1} R_{L-1}^{(k)} \tilde{g}_{L-2}^{(K)}(X_{\tilde{g}_{L-2}^{(K)}}) \times \lambda_{R_{L-1}^{(k)}} \lambda_{\tilde{g}_{L-2}^{(K)}} + b_{L-1} \right) \\ \tilde{h}_{L-1}^{(K)}(X_{\tilde{h}_{L-1}^{(K)}}) & = \sigma_{L-1} \left(\sum_{k=K_1+1}^K R_{L-1}^{(k)} \tilde{h}_{L-2}^{(K)}(X_{\tilde{h}_{L-2}^{(K)}}) \times \lambda_{R_{L-1}^{(k)}} \lambda_{\tilde{h}_{L-2}^{(K)}} \right) \\ X_{\tilde{g}_{L-1}^{(K)}} & = \tilde{g}_{L-2}^{(K)} \circ \dots \circ \tilde{g}_1^{(K)}(x) \\ X_{\tilde{h}_{L-1}^{(K)}} & = \tilde{h}_{L-2}^{(K)} \circ \dots \circ \tilde{h}_1^{(K)}(x) \end{cases} \quad (27)$$

The key element is the definition of $\tilde{g}_{L-1}^{(K)}$ and $\tilde{h}_{L-1}^{(K)}$, which are obtained by applying equation 32 two times, on $g_{L-2}^{(K)}$ and $h_{L-2}^{(K)}$ independently. This is detailed in Appendix E.

We showed that we can express $f^{(K)}$ as a sum of two quantized DNNs \tilde{g} and \tilde{h} . The first predictor \tilde{g} is equal to the expansion $f^{(K_1)}$ of f at order K_1 while \tilde{h} is equal to the expansion of $f^{(K)} - f^{(K_1)}$ at order $K - K_1$. This result can be extended to rewrite f as an ensemble of M predictors, by selecting K_1, \dots, K_M such that $\sum_{m=1}^M K_m = K$: in such a case, the M^{th} predictor will be the expansion of $f^{(K)} - f^{(\sum_{m=1}^{M-1} K_m)}$ at order K_M .

The proof of theorem B.3 follows from lemma B.4 and corollary B.5. We derive the exact formula for the upper bound U in the general case of L layers feed forward neural networks

$$\sum_{k=1}^K \|R_L^{(k)}\| \prod_{l=1}^{L-1} \sum_{k=K_1}^K \mathbb{E} \left[\left\| \tilde{h}_l^{(k)} \right\| \right] \lambda_{\tilde{h}_l^{(k)}} P \quad (28)$$

where $P = \left(1 - \mathbb{P} \left(f_l^{(K)} > 0 \cup \tilde{f}_l^{(K)} > 0 \right) \right)$. This is a consequence of the definition of the operator norm and the proposed ensembling. The approximation is obtained under the same assumptions and with the same arguments as provided in Corollary B.5.

C. Sparse Expansion Outperforms Standard Expansion

Lemma C.1. *Let f be a layer of real-valued weights W with a symmetric distribution. Then, for $K' < K$ two integers, we have:*

$$\text{Err} \left(R^{(1)} + \sum_{k=2}^{K'} R_{\gamma_1}^{(k)} \right) \geq \text{Err} \left(R^{(1)} + \sum_{k=2}^K R_{\gamma_2}^{(k)} \right) \quad (29)$$

where Err is the quantization error (i.e. the absolute difference between the quantized and original weights, as in Equation 6) and $K' \times \gamma_1 = K \times \gamma_2 = \beta$.

Table 6: Top1 Accuracy of MobileNet V2 on ImageNet for a expansion in int6 and $R_{50\%}^{(2)}$. We tested each strategy and the linear ascending (linear+) is the best performing one.

	const	linear+	linear -	adaptive
MobileNet (0.35)	55.15	59.46	33.69	58.19
MobileNet (0.5)	51.59	64.96	46.56	64.43
MobileNet (0.75)	66.31	69.10	55.78	68.92
MobileNet (1)	67.07	71.55	56.98	70.85
MobileNet (1.4)	72.55	74.05	69.38	73.15

Proof. Let's assume the layers outputs two channels. Then, we have $\gamma_1 = 1$ and $\gamma_2 = 0.5$. We simply need to prove the result for $k_1 = 2$ and $k_2 = 1$ as the result will extend naturally from this case. The idea of the proof consists in showing that using lower β values enables more possibilities of expansions which may lead to better performance. Let's note $(W)_1$ and $(W)_2$ the weights corresponding to the computation of the first and second output channels respectively. Using $\gamma_1 = 1$, the second order expansion correspond to either quantizing $(W)_1$ or $(W)_2$. Assume $(W)_1$ is chosen for $R_{\gamma_1}^{(2)}$. Then, $R_{\gamma_1}^{(3)}$ will either quantize the error from $(W)_2$ or further quantizes the error from $R_{\gamma_1}^{(2)}$. In the first case we end up with $R^{(1)} + \sum_{i=2}^{k_1} R_{\gamma_1}^{(i)} = R^{(1)} + \sum_{n=2}^{k_2} R_{\gamma_2}^{(i)}$. Otherwise, $\text{Err} \left(R^{(1)} + \sum_{i=2}^{k_1} R_{\gamma_1}^{(i)} \right) > \text{Err} \left(R^{(1)} + \sum_{i=2}^{k_2} R_{\gamma_2}^{(i)} \right)$. \square

D. Sparse Budget Split Across Layers

We split the budget over the layers by defining layer-wise thresholds γ^l such that $\sum_l |W_l| \gamma^l = \gamma \sum_l |W_l|$ where $|W_l|$ denotes the number of scalar parameters in layer l . The best tested strategy is a linear ascending function of l , *i.e.* $\gamma^l = al + \gamma^1$, $a > 0$:

$$\begin{cases} a = \frac{(1-\gamma) \sum_l |W_l|}{\sum_l l |W_l| - \sum_l |W_l|} \\ \gamma^1 = 1 - aL \\ \gamma^l = \text{clip}_0^1(al + \gamma^1) \end{cases} \quad (30)$$

where clip_0^1 is the clipping operator of bounds 0 and 1. This strategy gives more budget to the last layers which correspond to the largest layers. We validate the strategy choice by trying four options of selection of the (γ^l) from γ and comparing the results on MobileNets for ImageNet. The candidates are:

1. the constant strategy where $\gamma^l = \gamma$ for all l
2. the proposed linear ascending strategy (noted linear ascending or linear+) from equation 30 which puts more importance on the last layers
3. the linear descending strategy (noted linear descending or linear-) which, on the contrary, puts more importance on the first layers
4. a width-adaptive strategy which is derived from the number of neurons/channels for each layer, such that $\gamma^l = \gamma \frac{L|W_l|}{\sum_l |W_l|}$

We tested the performance of the method with a budgeted expansion $R_{50\%}^2$ in int6 (with order $k = 2$ and $\gamma = 50\%$). The results are listed in Table 6. We observe that the linear+ strategy is the best performing one: one possible explanation is that the first layers of a DNN typically have fewer values, thus are easier to quantize well.

E. Ensembling Protocol

Lemma A.1 and A.3 state that the first terms in the expansion, *i.e.* the lower values of k , are preponderant within the magnitude before the activation. Moreover, the activation functions traditionally used in DNNs (e.g. ReLU) satisfy $\sigma(x + \epsilon) \approx \sigma(x) + \sigma(\epsilon)$ when $|\epsilon| \rightarrow 0$. With respect to the proposed expansion, x corresponds to the first orders and ϵ to the terms of higher orders. In the case of two-layers networks, these properties allow us to break down the network in an

(approximately) equivalent ensemble of two networks, the first one containing the first, largest orders, and the second one containing the remaining ones.

E.1. Ensemble of two Layers DNNs

Let F be a feed-forward DNN with two layers f_1, f_2 and σ a piece-wise affine activation function (e.g. ReLU). Given $(R_1^{(k)})_{k=1\dots K}$ and b_1 the kernel and bias weights of the first layer $f_1^{(K)}$ respectively, we define the quantization expansion of residual errors $(R_1^{(k)})_{k \in \{1, \dots, K\}}$ of order K as in equation 7. Lemma A.1 states that the first terms in the sum, *i.e.* the lower values of k , are preponderant in the pre-activation term. Thus, there exists $K_1 < K$ such that $f_1^{(K)} \approx \tilde{f}_1^{(K)} = \tilde{f}_{1,1}^{(K)} + \tilde{f}_{1,2}^{(K)}$ with:

$$\begin{cases} \tilde{f}_{1,1}^{(K)} : x \mapsto \sigma \left(\sum_{k=1}^{K_1} R_1^{(k)} x^q \lambda_{R_1^{(k)}} \lambda_x + b_1 \right) \\ \tilde{f}_{1,2}^{(K)} : x \mapsto \sigma \left(\sum_{k=K_1+1}^K R_1^{(k)} x^q \lambda_{R_1^{(k)}} \lambda_x \right) \end{cases} \quad (31)$$

Furthermore $F^{(K)} : x \mapsto f_2^{(K)}(f_1^{(K)}(x))$. Let $R_2^{(k)}$ and b_2 respectively denote the kernel and bias weights of the second layer $f_2^{(K)}$. By linearity of the last layer, we have

$$\begin{aligned} F^{(K)} \approx \tilde{F}^{(K)} &= \sum_{k=1}^K R_2^{(k)} \tilde{f}_{1,1}^{(K)} \lambda_{R_2^{(k)}} \lambda_{\tilde{f}_{1,1}^{(K)}} + b_2 \\ &+ \sum_{k=1}^K R_2^{(k)} \tilde{f}_{1,2}^{(K)} \lambda_{R_2^{(k)}} \lambda_{\tilde{f}_{1,2}^{(K)}} \end{aligned} \quad (32)$$

Stemming from this formulation, we can express the quantized network $f^{(K)}$ as an ensemble of quantized neural networks which share a similar architecture, *i.e.* $F^{(K)} \approx \tilde{F}^{(K)} = \tilde{g}^{(K)} + \tilde{h}^{(K)}$. This defines the ensemble expansion from residual errors of order K .

E.2. Ensemble of more Layers DNNs

Similarly, we demonstrate by structural induction that a network with arbitrary number of layers L can be approximated by an ensemble expansion $\tilde{F}^{(K)}$ composed of M quantized networks, defined by the parameters K_1, \dots, K_M setting the size of each predictor, such that $K_1 + \dots + K_M = K$ (the total number of orders in the expansion).

We recall that $f_{L-1}^{(K)}(x) = \sigma_{L-1} \left(\sum_{k=1}^K R_{L-1}^{(k)} \lambda_{R_{L-1}^{(k)}} X_{f_{L-1}^{(K)}} + b_{L-1} \right)$. If we directly apply equation 31 then we get for a given $K_{L-1} < K$

$$X_{f_{L-1}^{(K)}} \mapsto \sigma_{L-1} \left(\sum_{k=1}^{K_{L-1}} R_{L-1}^{(k)} X_{f_{L-1}^{(K)}} \lambda_{X_{f_{L-1}^{(K)}}} \lambda_{R_{L-1}^{(k)}} + b_{L-1} \right) + \sum_{k=K_{L-1}+1}^K R_{L-1}^{(k)} X_{f_{L-1}^{(K)}} \lambda_{X_{f_{L-1}^{(K)}}} \lambda_{R_{L-1}^{(k)}} \quad (33)$$

However the two terms $X_{f_{L-1}^{(K)}(x)}$ inside and outside the activation function are not independent. Furthermore, the terms that compose $X_{f_{L-1}^{(K)}(x)}$, from equation 27, do not have the same range values, *i.e.* $\tilde{g}_{L-2}^{(K)}(X_{\tilde{g}_{L-2}^{(K)}}) \lambda_{\tilde{g}_{L-2}^{(K)}} >> \tilde{h}_{L-2}^{(K)}(X_{\tilde{h}_{L-2}^{(K)}}) \lambda_{\tilde{h}_{L-2}^{(K)}}$. We define the operation $*$ as follows

$$\begin{aligned} \tilde{f}_{L-1}^{(K)}(x) &= \sigma_{L-1} \left(\sum_{k=1}^{K_{L-1}} R_{L-1}^{(k)} \tilde{g}_{L-2}^{(K)}(X_{\tilde{g}_{L-2}^{(K)}}) \times \lambda_{R_{L-1}^{(k)}} \lambda_{\tilde{g}_{L-2}^{(K)}} + b_{L-1} \right) + \sum_{k=K_{L-1}+1}^K R_{L-1}^{(k)} \tilde{g}_{L-2}^{(K)}(X_{\tilde{g}_{L-2}^{(K)}}) \lambda_{R_{L-1}^{(k)}} \lambda_{\tilde{g}_{L-2}^{(K)}} \\ &+ \sigma_{L-1} \left(\sum_{k=1}^{K_{L-1}} R_{L-1}^{(k)} \tilde{h}_{L-2}^{(K)}(X_{\tilde{h}_{L-2}^{(K)}}) \times \lambda_{R_{L-1}^{(k)}} \lambda_{\tilde{h}_{L-2}^{(K)}} \right) + \sum_{k=K_{L-1}+1}^K R_{L-1}^{(k)} \tilde{h}_{L-2}^{(K)}(X_{\tilde{h}_{L-2}^{(K)}}) \lambda_{R_{L-1}^{(k)}} \lambda_{\tilde{h}_{L-2}^{(K)}} \end{aligned} \quad (34)$$

Now, we have two independent functions $\tilde{g}_{L-1}^{(K)}$ and $\tilde{h}_{L-1}^{(K)}$ such that $\tilde{f}_{L-1}^{(K)} = \tilde{g}_{L-1}^{(K)} + \tilde{h}_{L-1}^{(K)}$, these functions have independent

inputs and

$$\left\{ \begin{array}{l} \tilde{g}_{L-1}^{(K)}(X_{\tilde{g}_{L-2}^{(K)}}) = \sigma_{L-1} \left(\sum_{k=1}^{K_{L-1}} R_{L-1}^{(k)} \tilde{g}_{L-2}^{(K)}(X_{\tilde{g}_{L-2}^{(K)}}) \times \lambda_{R_{L-1}^{(k)}} \lambda_{\tilde{g}_{L-2}^{(K)}} + b_{L-1} \right) \\ \quad + \sum_{k=K_{L-1}+1}^K R_{L-1}^{(k)} \tilde{g}_{L-2}^{(K)}(X_{\tilde{g}_{L-2}^{(K)}}) \lambda_{R_{L-1}^{(k)}} \lambda_{\tilde{g}_{L-2}^{(K)}} \\ \tilde{h}_{L-1}^{(K)}(X_{\tilde{h}_{L-2}^{(K)}}) = \sigma_{L-1} \left(\sum_{k=1}^{K_{L-1}} R_{L-1}^{(k)} \tilde{h}_{L-2}^{(K)}(X_{\tilde{h}_{L-2}^{(K)}}) \times \lambda_{R_{L-1}^{(k)}} \lambda_{\tilde{h}_{L-2}^{(K)}} \right) \\ \quad + \sum_{k=K_{L-1}+1}^K R_{L-1}^{(k)} \tilde{h}_{L-2}^{(K)}(X_{\tilde{h}_{L-2}^{(K)}}) \lambda_{R_{L-1}^{(k)}} \lambda_{\tilde{h}_{L-2}^{(K)}} \end{array} \right. \quad (35)$$

This defines an iterative procedure in order to define our ensembling of expansions of residual errors for a feed-forward neural network f with any number L of layers.

To sum it up, the resulting predictors share an identical architecture up to their respective expansion order, defined by K_1 . The crucial difference comes from their weight values which correspond to different orders of expansion of the full-precision weights. This is also the case if we want ensembles of three or more predictors. In such instances, instead of only K_1 , we would have K_1, \dots, K_{m-1} for m predictors.

Consequently, every predictor shares the same architecture (without biases) up to their respective expansion order. For each $m = 1, \dots, M$, the m^{th} predictor corresponds to the residuals at orders $k \in \{\sum_{l=1}^{m-1} K_l + i \mid i \in \{1, \dots, K_m\}\}$. This ensemble approximation allows to more efficiently parallelize the computations across the expansion orders for improved runtimes. The method for computing the weights of the ensemble predictors is summarized in Algorithm 1. We provide insights on how to set the size of each weak predictor in Appendix L

Algorithm 1 Ensemble Expansion Algorithm

Require: trained DNN f with L layers, hyper-parameters : K_1, \dots, K_M and γ such that $K = K_1 + \dots + K_M = K$ and the budget $\beta = (K-1)\gamma$, operator Q
 initialize γ^l ► equation 30
for $m \in \{1, \dots, M\}$ **do**
 initialize $f_m^{(K_m)}$ as a clone of f with K_m kernels per layer
end for
for $l \in \{1, \dots, L\}$ **do**
 $W \leftarrow$ base kernel of layer l in f
 $W_{\text{acc}} \leftarrow 0$ accumulated quantization error
for $m \in \{1, \dots, M\}$ **do**
for $k \in \{1, \dots, K_m\}$ **do**
 $R_{\gamma^l}^{(k)} \leftarrow Q(W - W_{\text{acc}}) \mathbb{I}_{\gamma^l}^{(k)}$ ► equation 12
 set k^{th} kernel of layer l of $f_m^{(K_m)}$ with $R_{\gamma^l}^{(k)}$
 $W_{\text{acc}} \leftarrow W_{\text{acc}} + Q^{-1}(R_{\gamma^l}^{(k)})$
end for
end for
end for
end for
define $\tilde{f}^{(K)}$ as the sum of the $f_m^{(K)}$

F. Implementation Details and Datasets

We validate the proposed method on three challenging computer vision tasks which are commonly used for comparison of quantization methods. First, we evaluate on ImageNet (Deng et al., 2009) ($\approx 1.2\text{M}$ images train/50k test) classification. Second, we report results on object detection on Pascal VOC 2012 (Everingham et al., 2012) ($\approx 17\text{k}$ images in the test set). Third, we benchmark on image segmentation on CityScapes dataset (Cordts et al., 2016) (500 validation images).

In our experiments we used MobileNets (Sandler et al., 2018) and ResNets (He et al., 2016) on ImageNet. For Pascal VOC object detection we employed an SSD (Liu et al., 2016) architecture with MobileNet backbone. On CityScapes we

Table 7: Processing time on an Intel(R) Core(TM) i9-9900K CPU @ 3.60GHz of the proposed method for different configurations and architectures trained on ImageNet and a quantization in TNN. We note ‘m’ for minutes and ‘s’ for seconds.

k	ensembling	ResNet 152	MobileNet v2 (1.4)
1	✗	0.32s	0.12s
2	✗	0.43s	0.13s
2	✓	0.43s	0.13s
7	✗	0.90s	0.51s
7	✓	0.92s	0.51s

Table 8: Comparison at equivalent bit-width (*i.e.* no-parallelization) with existing methods in W8/A8 and REx with W2/A2 with $K = 4$.

DNN	method	year	bits	Acc	DNN	method	year	bits	Acc
full-precision					full-precision				
ResNet 50	DFQ	ICCV 2019	8	75.45	MobNet v2	DFQ	ICCV 2019	8	70.92
	ZeroQ	CVPR 2020	8	75.89		SQuant	ICLR 2022	8	71.68
	DSG	CVPR 2021	8	75.87		REx	-	400% $\times 2$	71.65
	GDFQ	ECCV 2020	8	75.71	full-precision				
	SQuant	ICLR 2022	8	76.04	EffNet B0	DFQ	ICCV 2019	8	76.89
	SPIQ	WACV 2023	8	76.15		SQuant	ICLR 2022	8	76.93
	REx	-	400% $\times 2$	76.15		REx	-	400% $\times 2$	76.95

used DeepLab V3+ (Chen et al., 2018) with MobileNet backbone. We also test our method on VGG 16 (Simonyan & Zisserman, 2014) and transformers such as BERT model (Devlin et al., 2018) on GLUE (Wang et al., 2018)

In our experiments, the inputs and activations are quantized using the same method as Nagel et al. (2019). The number of bit-wise operation in our evaluation metric is discussed in Appendix H.

For SQuant (Cong et al., 2022), we use our own implementation which achieve different accuracy results due to different initial accuracies for baseline models. As for ZeroQ (Cai et al., 2020), we use results provided by SQuant (Cong et al., 2022). Similarly to prior work (Meller et al., 2019; Nagel et al., 2019; Cong et al., 2022), we denote W/A- the quantization setup (number of bits for weight quantization and number of bit for activation quantization).

We used Tensorflow implementations of the baseline models from the official repository when possible or other publicly available resources when necessary. MobileNets and ResNets for ImageNet come from tensorflow models [zoo](#). In object detection, we tested the SSD model with a MobileNet backbone from [Manish’s git repository](#). Finally, in image semantic segmentation, the DeepLab V3+ model came from [Bonlime’s git repository](#).

The networks pre-trained weights provide standard baseline accuracies on each tasks. The computations of the residues as well as the work performed on the weights were done using the Numpy python’s library. As listed in Table 7, the creation of the quantized model takes less than a second for a MobileNet V2 as well as for a ResNet 152 without any optimization of the quantization process. These results were obtained using an Intel(R) Core(TM) i9-9900K CPU @ 3.60GHz.

G. Other Results on ConvNets

G.1. More Results on ImageNet

In the following sections, we show that REx is also very flexible and can be straightforwardly applied to other computer vision tasks, e.g. object detection and semantic segmentation.

G.2. Object Detection

In Fig 6, we report the performance of REx (as well as DFQ (Nagel et al., 2019) for int8 quantization) using SSD-MobileNet as a base architecture for object detection. Overall, we observe a similar trend as in Section 4.3: REx reaches significantly lower numbers of bit-wise operations than the naive baseline ($R_{\gamma=100\%}^{k=1}$) and state-of-the-art DFQ (Nagel et al., 2019) while preserving the full model accuracy, using either int4, int3 or ternary quantization. Also, once again, the best results are obtained using ternary quantization with high orders (e.g. $k = 8$) and sparse residuals (e.g. $\gamma = 25\%$): as such, the

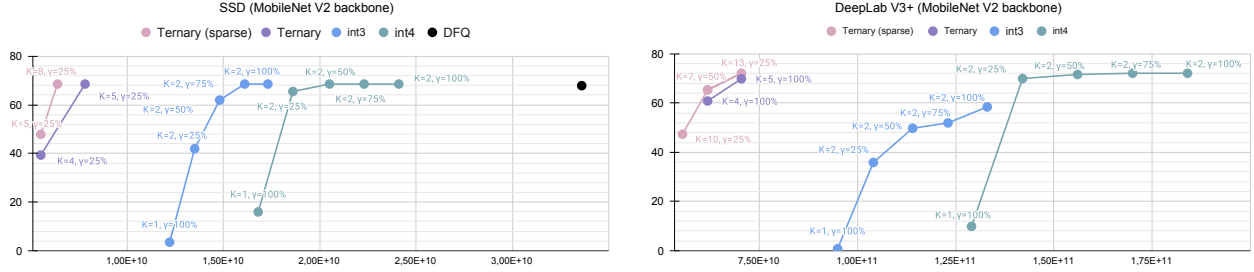


Figure 6: (a) Mean average precision (mAP) of a SSD with MobileNet V2 backbone on Pascal VOC for object detection. We add the performance of a data-free quantization solution, DFQ (Nagel et al., 2019) for comparison. (b) Mean intersection over union (mIoU) of a DeepLab V3+ with MobileNet V2 backbone on CityScapes for semantic segmentation.

mAP of the best tested configuration, $R_{25\%}^{(8)}$, reaches 68.6% for $6.38e^9$ bit-wise operations, vs. 67.9% for $3.36e^{10}$ bit-wise operations for DFQ (Nagel et al., 2019).

G.3. Semantic Segmentation

In Fig 6, we report the performance of REx for image segmentation using a DeepLab v3+ architecture. Similarly to the previous tasks, REx is able to very efficiently quantize a semantic segmentation network, whether it is in int4 or higher (where order 2 is sufficient to reach the full precision mIoU), or in int3/ternary quantization. In the latter case, once again, it is better to use sparse, high order expansions: for instance, we were able to retrieve the full accuracy using $R_{50\%}^{(9)}$ and ternary quantization, dividing by 10 the number of bit-wise operations as compared to the original model. This demonstrates the robustness of REx to the task and architecture.

H. Operation Head-count

Let W be the real-valued weights of a $d \times d$ convolutional layer on input feature maps of shape $D \times D \times n_i$ and n_o outputs and stride s . Then the convolutional product requires $d^2 \frac{D^2}{s^2} n_i n_o$ floating point multiplications. The quantized layer requires two rescaling operations (for the quantization of the inputs and the Q^{-1} operation) and an int- b convolution, i.e. $n_i D^2 + \frac{D^2}{s^2} n_o$ floating point multiplications and $d^2 \frac{D^2}{s^2} n_i n_o$ int- b multiplications. Note that the number of additions remains unchanged. According to Klarreich (2019) the lowest complexity for b -digits scalar multiplication is $o(b \log(b))$ bit operations. This is theoretically achieved using Harvey-Hoeven algorithm (also the asymptotic bound has yet to be proved). We use this value as it is the least favorable setup for the proposed method. As a consequence the number O_{original} bit operations required for the original layer, $O_{R^{(1)}}$ the number of bit operations for the naively quantized layer and $O_{R^{(k)}}$ for the i^{th} order residual quantization expansion are

$$\begin{cases} O_{\text{original}} = D^2 \frac{d^2 n_i n_o}{s^2} 32 \log(32) \\ O_{R^{(1)}} = D^2 \left[(n_i + \frac{n_o}{s^2}) 32 \log(32) + \frac{d^2 n_i n_o}{s^2} b \log(b) \right] \\ O_{R^{(k-1)}} = D^2 \left[(n_i + \frac{n_o}{s^2}) 32 \log(32) + k \frac{d^2 n_i n_o}{s^2} b \log(b) \right] \end{cases} \quad (36)$$

Using this result we can estimate the maximum order of expansion before which the number of operations in $f^{(k)}$ exceeds the O_{baseline} . Note that in the case of fully-connected layers, $D = 1$, $s = 1$ and $d = 1$. In the following section, we use the induced metric of accuracy with respect to the total number of bit-wise operations performed by the DNN on a single input. This metric doesn't consider the fact that the added operations can be performed in parallel.

I. Developments and Binary Representation

Let w_1 and w_2 be two different scalar weights associated to the same neuron. We note (r_1^k) and (r_2^k) their respective quantized developments, then

$$\begin{cases} w_1 \simeq \sum_{k=1}^K r_1^k \times \lambda_k \\ w_2 \simeq \sum_{k=1}^K r_2^k \times \lambda_k \end{cases} \quad (37)$$

Table 9: Top1 accuracy on ImageNet for ternary quantization of ResNet 50 and MobileNet v2. We tested different depth N of expansion and the corresponding proportion γ in order to have a fixed budget β . The experimental results confirm Lemma C.1.

Model	(N, γ)	β	accuracy
ResNet 50	(5, 50%)	2.5×10^{10}	16.55
ResNet 50	(9, 25%)	2.5×10^{10}	18.75
ResNet 50	(21, 10%)	2.5×10^{10}	20.05
ResNet 50	(41, 5%)	2.5×10^{10}	20.05
ResNet 50	(4, 100%)	3.2×10^{10}	65.63
ResNet 50	(5, 75%)	3.2×10^{10}	69.53
ResNet 50	(7, 50%)	3.2×10^{10}	76.15
ResNet 50	(13, 25%)	3.2×10^{10}	76.15
MobileNet v2	(7, 50%)	4.3×10^9	6.91
MobileNet v2	(13, 25%)	4.3×10^9	7.66
MobileNet v2	(30, 10%)	4.3×10^9	9.55
MobileNet v2	(60, 5%)	4.3×10^9	9.58
MobileNet v2	(5, 100%)	4.9×10^9	58.83
MobileNet v2	(9, 50%)	4.9×10^9	62.31
MobileNet v2	(17, 25%)	4.9×10^9	62.50
MobileNet v2	(41, 10%)	4.9×10^9	62.50

with the λ_k their corresponding rescaling factors. Assuming the quantizing is binary *i.e.* $b = 2$ and $r_i^k \in \{0, 1\}$ or $r_i^k \in \{-1, 1\}$. We want to discuss the influence of the choice between $\{0, 1\}$ and $\{-1, 1\}$ on the effectiveness of the development method. To draw a comparison we measure how fine-grained the representations are which corresponds to the smallest value $|w_1 - w_2|$ can take. From equation 37, we deduce

$$\begin{cases} r_i^k \in \{0, 1\} & \Rightarrow |w_1 - w_2| = \sum_{k=1}^K |\lambda_k| \mathbb{1}_{r_1^k \neq r_2^k} \\ r_i^k \in \{-1, 1\} & \Rightarrow |w_1 - w_2| = \sum_{k=1}^K 2|\lambda_k| \mathbb{1}_{r_1^k \neq r_2^k} \end{cases} \quad (38)$$

Consequently, the representation $\{0, 1\}$ shall be privileged in the context of the development of residual errors which goes against standard binarization using sign function.. This is a limitation of the current method as $\{0, 1\}$ forces us to alternate positive and negative values of λ which is equivalent to splitting the positive and negative terms in a ternary development. For this reason the binary representation may only be slightly better than the ternary.

Furthermore, current state-of-the-art in binary quantization doesn't actually fully quantize in binary for three reasons. First, padding is still defined as zeros while binary values are supposed to be $\{-1, 1\}$. Second, binarization removes the most important value (zero) and thus requires skip connections in 4 bits (Zhang et al., 2022). Third, the first and last layers are maintained in W8/A8.

J. On the limit value of K

In lemma C.1, we stated, for a given budget β , the higher the value of K the lower the error. based on this result one may naively set γ to its lowest non-zero possible value, *i.e.* $\gamma = \frac{1}{|W|}$ where $|W|$ is the total number of weights in f . However, Table 9 we show that not only the error decreases when K increases but we also show its asymptotic behavior with a convergence for $K \approx 13 \pm 3$.

We want to put the emphasis on a counter intuitive aspect of our theoretical results. This asymptotic behavior is not a direct result of the exponential convergence demonstrated in lemma A.2 and A.3. In these lemmas, we show that for an increasing K and a similarly increasing budget the convergence to 0 is exponential. In lemma C.1, we show that for a given budget the higher K the better. However, this is not enough to conclude that given a fixed β the convergence with respect to K is exponential to K . Furthermore depending on the budget β , in lemma C.1 the limit is not necessarily 0. The empirical results from Table 9 demonstrate that in practice the convergence is also fast when the budget is fixed.

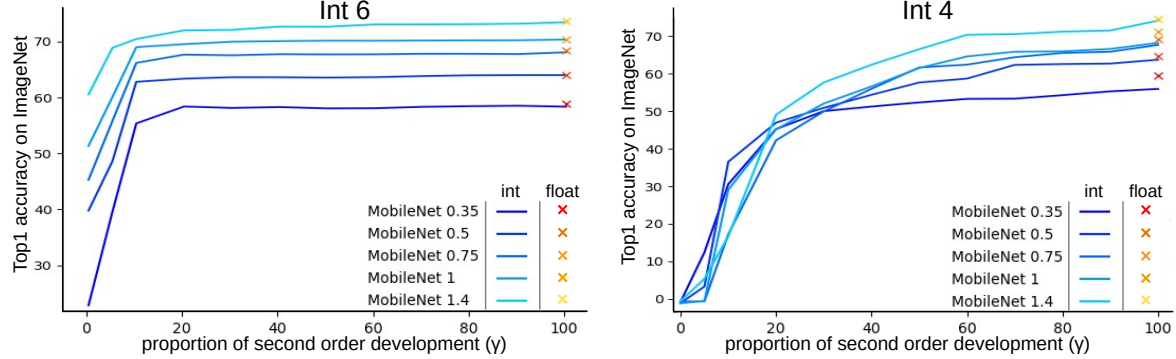


Figure 7: The top1 accuracy of MobileNets on ImageNet quantized in int6 (left) and int4 (right) as a function of γ for $k = 2$. We observe an immediate boost ($\gamma < 10\%$), especially in int6. Thus, the expansion can be used efficiently at a low overhead cost.

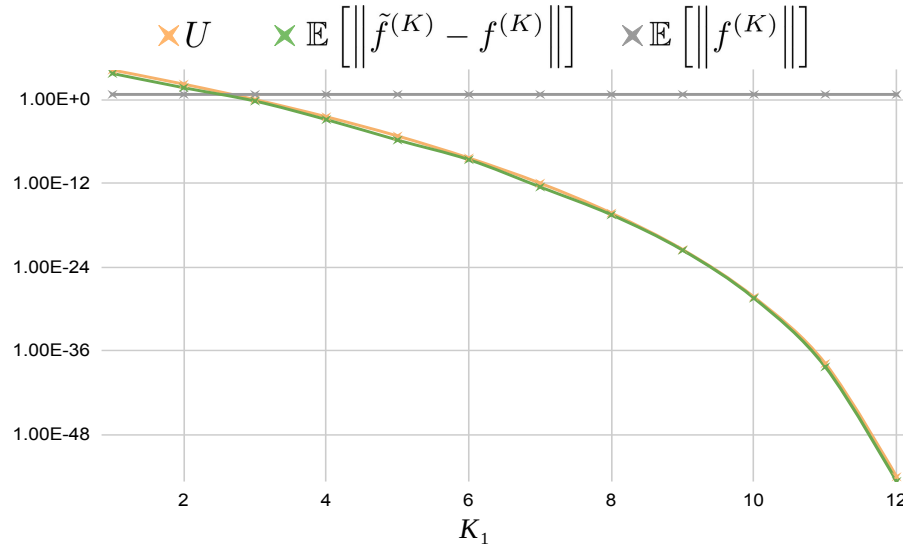


Figure 8: Comparison between the expected empirical error from ensembling $\mathbb{E}[\|f^{(K)} - \tilde{f}^{(K)}\|]$ (green) and its upper bound U (Lemma B.3, orange) for different values of K_1 on a ResNet 50 trained on ImageNet and quantized with ternary values and $K = 13$, $\gamma = 25\%$. We also plot the reference $\mathbb{E}[\|f^{(K)}\|]$ (grey).

K. The Robustness to the Value of γ

the Performance boost due to the group-sparsity expansion is immediate, *i.e.* even for small values of γ . This can be seen in Figure 7, where we show for different bit widths (int6 and int4) the influence of γ on the accuracy of several MobileNet V2 architectures (with various width multipliers) on ImageNet. In int4, the accuracy reaches its asymptotic convergence for $\gamma \approx 50\%$ but large improvements are already made for values below 20%. This is even more impressive in int6 where the accuracy is restored with $\gamma \approx 25\%$ and a significant increase can be observed for values below 10%. Note that under 20% the computation overhead is negligible.

L. How to set predictors size

We consider quantized expansions of networks with M predictors such that $\sum_{m=1}^M K_m = K$ (K_1 is the number of orders in the first predictor of the ensemble) and γ the sparsity factor. The larger K_1 , the lower the difference between the ensemble $\tilde{f}^{(K)}$ and the developed network $f^{(K)}$. Conversely, the more balanced the elements of the ensemble, the more runtime-efficient the ensemble: thus, K_1 have to be fixed carefully so that the ensemble shall be faster than the developed network, without accuracy loss. Fortunately, the accuracy behaviour w.r.t. the value of K_1 can be estimated from the values of the upper bound U (Lemma B.3) on the expected error from ensembling $\mathbb{E}[\|f^{(K)} - \tilde{f}^{(K)}\|]$. As illustrated on Figure 8 in the

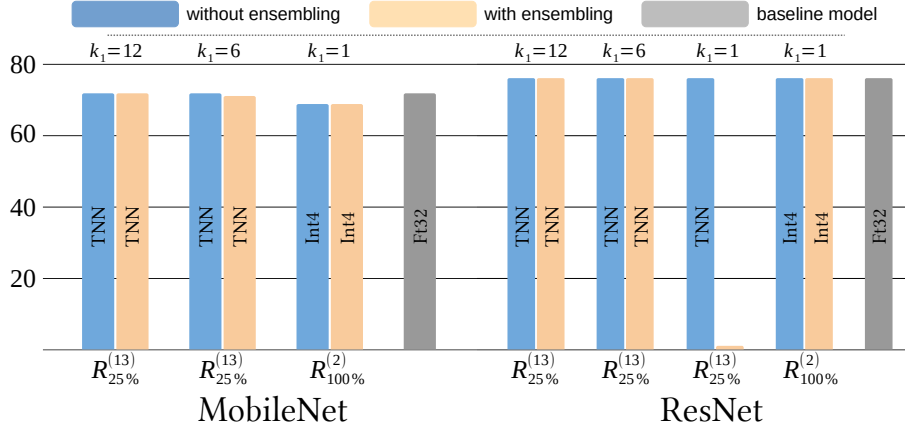


Figure 9: Comparison between ensemble expansion $\tilde{f}^{(K)}$ (in orange) and regular expansion $f^{(K)}$ (blue) on ImageNet. We test different bit representations, namely ternary (TNN) and int4 as well as different values for K_1 . Except for very low values the ratio K_1/K , we observe the robustness of the ensembling method.

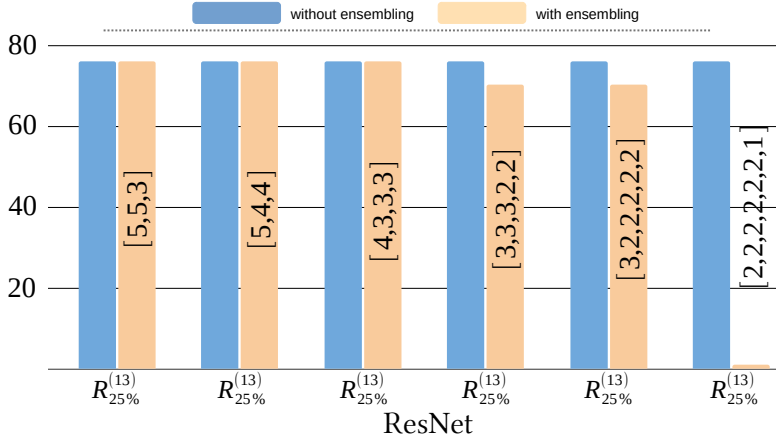


Figure 10: Comparison between TNN ensemble expansion $\tilde{f}^{(K)}$ (in orange) and regular expansion $f^{(K)}$ (blue) on ImageNet.

case of ternary quantization, this upper bound is tight and collapses more than exponentially fast w.r.t. K_1 . For instance, if $K_1 \leq 2$, U is significantly larger than the amplitude of the logits $\mathbb{E}[\|f^{(K)}\|]$ and the accuracy is at risk of collapsing. When U vanishes compared to $\mathbb{E}[\|f^{(K)}\|]$, the ensemble and regular expansions are guaranteed to be almost identical, and the accuracy is preserved. Thus, we can compare the upper bound U and the empirical norm of the logits from the expansion $\mathbb{E}[\|f^{(K)}\|]$ to assess the validity of an ensemble. Plus, $\mathbb{E}[\|f^{(K)}\|]$ can be estimated using statistics from the last batch norm layers to allow for a fully data-free criterion.

With this in mind, in Figure 9 we compare the top-1 accuracies of $\tilde{f}^{(K)}$ and $f^{(K)}$ for different architectures (MobileNet v2 and ResNet 50) and quantization configurations. The ensemble expansion systematically matches the accuracy of the developed network in terms of accuracy, except in the case of ternary quantization when $K_1 = 1$. This is remarkable as ensembling significantly decreases the inference time with a two predictors configuration.

Figure 10 shows the results obtained with larger ensembles of smaller quantized predictors, *i.e.* with $M > 2$. We observe the full preservation of the accuracy of the developed network as long as $K_1 \geq 4$ and a loss of 6 points for balanced ensembles of 5 – 6 predictors and $K_1 = 3$. Here again, with $M = 7$ and $K_1 = 2$, the accuracy is very low, as predicted by 8. To sum it up, ensembling developed networks allows to significantly decrease the inference time, with theoretical guarantees on the accuracy preservation.

Finally, Table 10 shows the runtime of a ResNet 50 for a full evaluation on ImageNet validation set (50,000 images). We tested the models on different devices (CPU/GPU) using a fixed budget $\beta = 7$ and order $K = 8$, and compared ensembles

Table 10: Comparison of the evaluation time in seconds of a ResNet 50 over the validation set of ImageNet using a expansion of order $k = 8$ with ensembling of m predictors $m \in \{1, 2, 3, 4\}$. We distinguish the setups by reporting the values of $[K_1, \dots, K_m]$.

device	[8]	[4, 4]	[3, 3, 2]	[2, 2, 2, 2]	[1]
expansion	✓	✓	✓	✓	✗
ensembling	✗	✓	✓	✓	✗
Intel(R) i9-9900K	215	54	26	26	25
Ryzen 3960X	122	30	23	22	22
RTX 2070	13	8	5	5	5
RTX 3090	11	7	4	4	4

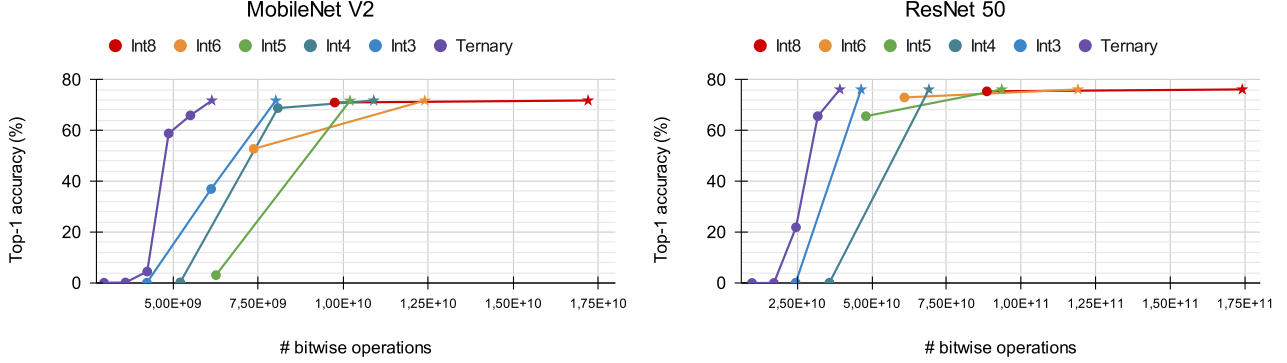


Figure 11: ImageNet top1 accuracy of quantized MobileNet V2 and ResNet 50. We compare the expansions at orders 1 – 3 for int3, int4, int5, int6 and int8 quantization as well as the ternary quantization of higher orders ($K = 5, 6$ respectively for ResNet 50 and MobileNet V2, in purple).

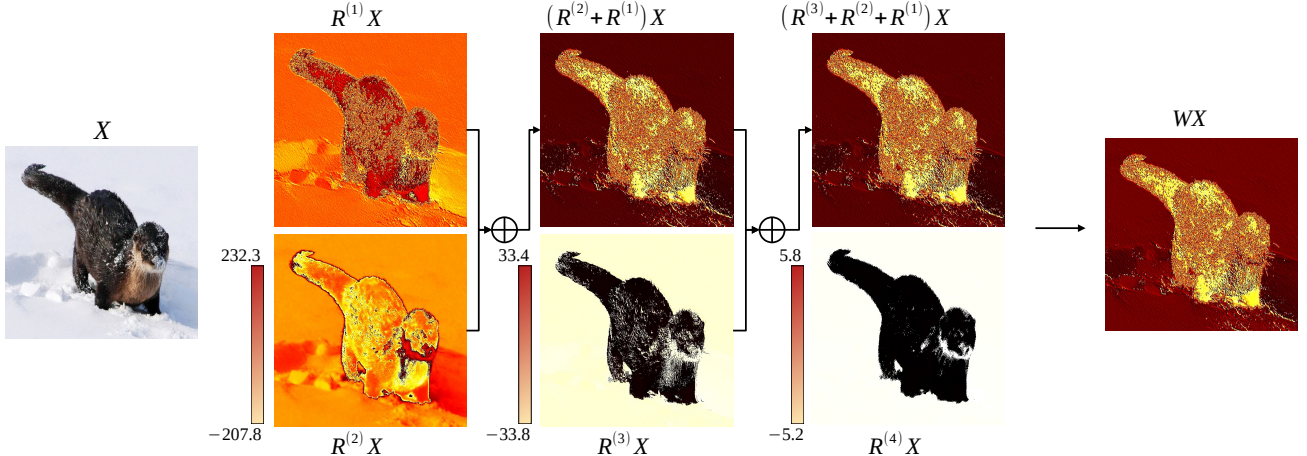


Figure 12: Convergence towards full-precision features WX of the proposed expansion of weights of the first layer of a ResNet 50 quantized in int3. The scales decrease exponentially fast to zero.

expansions (with 2 [4, 4], 3 [3, 3, 2] and 4 [2, 2, 2, 2] predictors). On each device, the ensembles are up to 10 times faster than the baseline expansion.

M. Detailed Trade-Offs of the Expansions

Fig 11 illustrates the trade-off between the accuracy on ImageNet of a ResNet 50 and a MobileNet v2 and the number of bitwise operations. We report different expansion orders K (no sparsity) and number of bits b for standard bit representations ($b \geq 3$). In most cases, we observe a systematic convergence to the full-precision accuracy with $K = 2$.

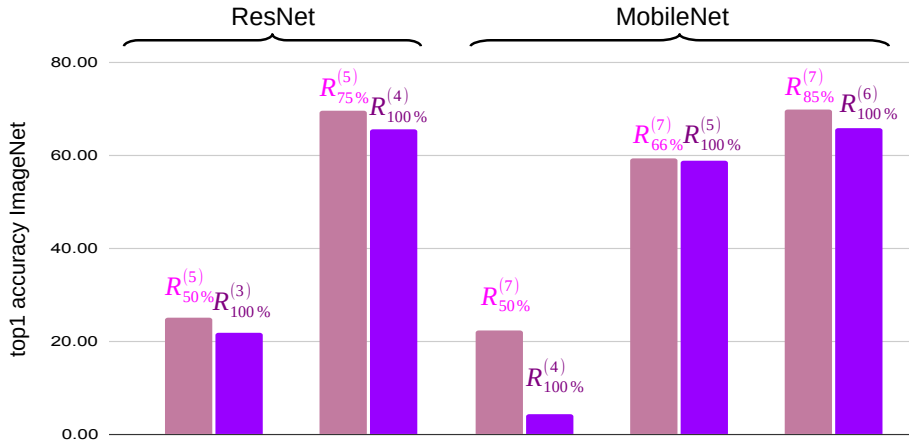


Figure 13: ImageNet top1 accuracy of MobileNet V2 and ResNet 50, and comparison between full expansions and sparse expansion of higher orders, with similar budgets for ternary quantization. In every case, the sparse expansion of higher orders achieves a better accuracy.

On the more challenging benchmark for quantization methods such as 4 bits or ternary quantization (TNN), where the quantized weights can either take the values $-1, 0$ or 1 , higher values of K are required in order to reach the full-precision accuracy. This is also illustrated on Fig 11. Here again, the ternary-quantized models reach the full precision With $K = 5, 6$ for ResNet 50 and MobileNet v2 respectively. This is an empirical validation of the exponential convergence w.r.t. the expansion order, as stated in lemma A.1. This is also illustrated in Fig 12 with the convergence of feature maps to the full precision features with respect to the order of expansion. The added elements have a decreasing impact. However, while this setting already constitutes a good trade-off between accuracy and number of bit-wise operations, using such high order expansions remains computationally expensive, without sparsity nor ensembling, as compared to a naive quantization scheme, *i.e.* using $K = 1$. This is addressed by budgeted sparsity and ensemble expansions.

As stated in Lemma C.1, given a specific budget, using higher order (high K) sparse (low γ) residual expansions allows to find a better accuracy vs. number of bit-wise operations trade-off. Intuitively, the lower b the bit width, the more fine-grained the possible budgets: therefore, REx performs better and is more flexible using low bit width such as ternary weights with sparse higher order expansions. For instance, on MobileNet, any values of $\beta = (K - 1)\gamma$ greater than 3 will reach the full-precision accuracy with int4 representations. Similarly, on ResNet, any value of β greater than 3.5 allows to reach the full-precision accuracy.

Fig 13 draws a comparison between full orders and sparse (higher) orders for an equivalent budget in case of ternary quantization: in every case, the sparse, high-order expansion achieves greater accuracy than the full, lower-order one: e.g. ResNet with $R_{75\%}^{(5)}$ achieves 69.53% top-1 accuracy vs 65.63% for $R_{100\%}^{(4)}$; MobileNet with $R_{85\%}^{(7)}$ achieves 69.94% top-1 accuracy vs 65.94% for $R_{100\%}^{(6)}$. We propose a more in-depth study of the behavior of the quantized neural networks w.r.t. extreme values of γ (below 0.1) in Appendix K. Overall, the budgeted expansion significantly improves the ternary quantization. It reduces by 15% and 20% the budget as compared to the standard expansion, in order to reach full-precision accuracy on ResNet 50 and MobileNet V2.

Fig 14, complements Fig 2. For instance, on ResNet 50, we need to use W6/A6 quantization in order to reach a decent 86.18% relative accuracy, *i.e.* 65.625% top1 accuracy. Meanwhile, the standard expansion reaches the full-precision accuracy (76.15%) at a 18.21% lower inference cost. Furthermore, the sparse expansion manages to further reduce the inference cost by an other 8.84%.

N. Pre-Processing Time

As shown on Table 11, in terms of quantization processing time, methods relying on data generation (DG) such as ZeroQ (Cai et al., 2020), DSG (Zhang et al., 2021), GDFQ (Xu et al., 2020) and MixMix (Li et al., 2021b) are slow as they usually require many forward-backward passes to quantize a trained neural network. REx, on the other hand, is very fast in addition to being better at preserving the original model accuracy with theoretical control over the error introduced by

REx: Data-Free Residual Quantization Error Expansion

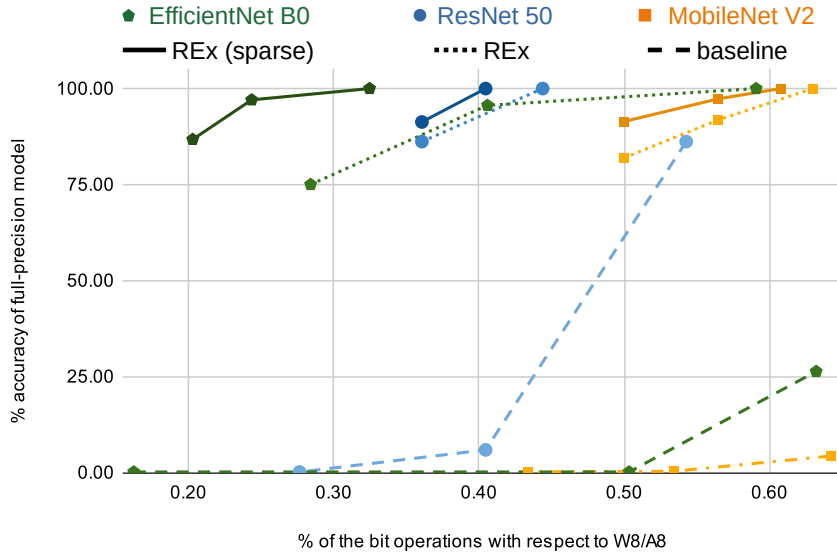


Figure 14: Accuracy vs. inference time, for EfficientNet B0. The higher (accuracy) and the further to the left (inference cost) the better. The dashed lines show the baseline results with W3/A3, W4/A4 and W6/A6 quantization. The fine-dashed lines show the performance of REx, and the plain lines show REx (sparse) both in ternary quantization. REx, and *a fortiori* the sparse version, enables better trade-offs.

Table 11: REx, MixMix, GDFQ and ZeroQ 4-bit quantization time in seconds. REx was quantized such that full-precision accuracy is reached.

Model	ZeroQ	GDFQ	MixMix	REx
ResNet 50	92.1	11.10^3	18.10^3	<1
ResNet 101	164.0	18.10^3	25.10^3	<1
ResNet 152	246.4	24.10^3	30.10^3	1.1
MobileNet V2 (0.35)	27.4	3.10^3	6.10^3	<1
MobileNet V2 (1)	37.9	7.10^3	12.10^3	<1

Table 12: Accuracy for ResNet 50 on ImageNet. REx (with ensembling) achieves excellent accuracy for both standard and low-bit quantization, more-so using high-order sparse expansions, vastly outperforming previous state-of-the-art data-free quantization approaches such as OCS, DFQ, SQNR and SQuant, and even approaches that require fine-tuning as MixMix, ZeroQ, DSG and GDFQ.

method	year	no-DG	b	accuracy
	full-precision			76.15
OCS	ICML 2019	✓	8	75.70
DFQ	ICCV 2019	✓	8	76.00
SQNR	ICML 2019	✓	8	75.90
ZeroQ	CVPR 2020	✗	8	75.89
DSG	CVPR 2021	✗	8	75.87
SQuant	ICLR 2022	✓	8	76.04
REx	-	✓	8	76.15

method	year	no-DG	b	accuracy
	full-precision			76.15
OCS	ICML 2019	✓	4	0.1
DSG	CVPR 2021	✗	4	23.10
GDFQ	ECCV 2020	✗	4	55.65
SQuant	ICLR 2022	✓	4	68.60
MixMix	CVPR 2021	✗	4	74.58
AIT	CVPR 2022	✗	4	66.47
REx	-	✓	4	76.13

quantization.

O. More Parallelization Results

In Table 12, we compare REx and the state-of-the-art data-free quantization methods OCS (Zhao et al., 2019), DFQ (Nagel et al., 2019), SQNR (Meller et al., 2019) and methods that involve synthetic data, such as ZeroQ (Cai et al., 2020), DSG (Zhang et al., 2021), GDFQ (Xu et al., 2020) and MixMix (Li et al., 2021b). We report results on int8 and int4 quantization: for the former case, we use order 2 residual expansion without ensembling (as the inference time are equivalent with the

baseline model, see Fig 3). For int4 quantization, we report results at order 4 with an ensemble of 2 predictors, each containing two orders, *i.e.* $K_1 = K_2 = 2$. Using this setup ensures that the inference run-times are comparable (see Fig 3).

First, given a budget of bit-wise operations that achieves equivalent expected run-time (Fig 3), REx can achieve higher accuracy than existing approaches: *e.g.* on both MobileNet V2 and ResNet, in int4, REx outperforms SQuant (Cong et al., 2022), the best data-free method that does not involve data-generation (DG), by 16.3 points and 7.5 respectively. Note that other methods such as OCS (also involving structural changes in the neural network architecture) considerably underperforms, especially on int4 where the accuracy drops to 0.1. REx, however, fully preserves the floating point accuracy.

Second, REx even outperforms the impressive (yet time consuming) data-generation (DG) based methods such as ZeroQ (Cai et al., 2020), DSG (Zhang et al., 2021), GDFQ (Xu et al., 2020) and MixMix (Li et al., 2021b). The difference is more noticeable on low bit quantization, *e.g.* $b = 4$. Nevertheless, REx improves the accuracy on this benchmark by 6.35% top-1 accuracy. Similarly, to the results on MobileNet V2, on ResNet-50, REx reaches accuracies very close to the full precision model (76.13), significantly outperforming its closest contender, MixMix (74.58).